

Final Draft
of the original manuscript:

Khan, M.M.; Filiz, V.; Bengtson, G.; Shishatskiy, S.; Rahman, M.M.;
Lillepaerg, J.; Abetz, V.:

**Enhanced Gas Permeability by Fabricating Mixed Matrix
Membranes of Functionalized Multiwalled Carbon Nanotubes
and Polymers of Intrinsic Microporosity (PIM)**

In: Journal of Membrane Science (2013) Elsevier

DOI: 10.1016/j.memsci.2013.02.032

Enhanced Gas Permeability by Fabricating Mixed Matrix Membranes of Functionalized Multiwalled Carbon Nanotubes and Polymers of Intrinsic Microporosity (PIM)

Muntazim Munir Khan, Volkan Filiz*, Gisela Bengtson, Sergey Shishatskiy, Md.Mushfequr Rahman, Jelena Lillepaerg, Volker Abetz*

Helmholtz-Zentrum Geesthacht, Institute of Polymer Research, Max-Planck-Str. 1, 21502 Geesthacht, Germany

* Corresponding authors. Tel.: +49 (0)4152 87 2461; Fax: +49 (0)4152 87 2499

E-mail addresses: volkan.filiz@hzg.de; volker.abetz@hzg.de

Abstract:

In this study, mixed matrix membranes (MMM) consisting of multi-walled carbon nanotubes (MWCNTs) embedded in PIM-1 matrix have been fabricated via solution casting method and their gas transport properties are investigated. The MWCNTs were chemically functionalized with polyethylene glycol (PEG) for a better dispersion in the polymer matrix. The effect of functionalized MWCNTs (f-MWCNTs) loading on gas permeation properties of the MMM were investigated by varying the MWCNTs loading in a PIM-1 matrix from 0.5 – 3.0 wt %. The derived MMM were characterized by scanning electron microscopy (SEM), thermogravimetric analysis (TGA) and single gas permeation tests. Gas permeation measurements showed that MMM incorporated with modified and non-modified CNTs exhibited different gas separation performance. The f-MWCNT MMM show better performance compared to MMM with non-modified CNTs in terms of dispersion and permeability at 2 wt% f-MWCNTs loading without sacrificing selectivity. According to diffusivity and solubility data derived from the time-lag method, the PEG chains on MWCNTs show interaction with CO₂ as indicated by an increase of the solubility of the polar gas and a reduction of the solubility of non-polar gas, which is advantageous for CO₂/N₂ separation. The mechanical properties and experimental sorption isotherms of CO₂ and N₂ of the f-MWCNTs/PIM MMM were enhanced as well.

Keywords

Mixed matrix membrane, Multi-walled carbon nanotubes, Polymer of intrinsic microporosity

1. Introduction:

Improvements in the performance of polymeric materials for gas separation membranes have been made during the last two decades [1-6], and understanding of the relationship between the polymer structure and gas transport properties of polymeric membranes has been greatly advanced [2, 3]. Despite these advantages and progresses, polymeric membranes are restricted by the trade-off trend between gas permeability and selectivity, as shown by Robeson [7]. Most of the researchers have paid special attention to the relationship between polymer structure and gas separation properties in order to improve membrane performance both in permeability and selectivity. The permeability of a polymeric membrane is mainly controlled by the chain mobility and the fractional free volume of the polymer structure.

The introduction of rigid fillers having particle size close to the characteristic size of the macromolecules forming the selective polymer film may be the best technique to improve gas permeability by hindering molecular chain packing and increasing free volume. Therefore mixed matrix membranes (MMM) defined as the synergistic combination of organic polymers with inorganic nanofillers (permeable, as well as impermeable) dispersed at nanometre level have been studied as an alternative approach to solve the trade-off problem of polymeric membrane in gas separation [8, 9]. Compared to pure polymer membranes, many polymer-inorganic (such as silica and titania) nanocomposite membranes show higher permeabilities without sacrificing gas selectivity [10-14]. Among them, carbon nanotube (CNT)-based MMM have been developed due to their enhanced tensile modulus and stress at break [15-17]. Molecular dynamics simulation predicted that the transport of light gases inside CNTs should be orders of magnitude faster than in any other material, in fact as fast as in gases [18, 19] due to inherent smoothness of the nanotube. Experimental studies confirmed that carbon nanotubes as the inorganic nanofillers in nanocomposite membrane did facilitate gas permeability compared to pure polymeric counterparts.

For instance, Kim et al. [20] reported on the addition of CNTs to poly(imide siloxane) membranes which resulted in increased O₂, N₂ and CH₄ permeability. Cong et al.[21] prepared the brominated poly(2, 6-diphenyl-1, 4-phenylene oxide) composite membrane with SWCNTs or MWCNTs and found that low concentration of CNTs addition increases the gas permeability without sacrificing selectivity. Weng et al. [22] fabricated a MWCNTs/ Poly(bisphenol A-co-4-nitrophthalic anhydride-co-1,3-phenylene diamine) PBNPI membrane.

In their results, both the permeabilities and the selectivities of H₂, CO₂ and CH₄ improved significantly at high MWCNTs concentrations (>5 wt%). Pinnau et al. reported an unexpected increase of gas permeability without loss of gas selectivity in a series of high-free-volume glassy polymers whereby inorganic non-porous nanoparticles, such as fumed silica or carbon black, were incorporated into the polymeric matrix [23]. Based on these investigations, one can conclude that the interaction between polymer matrix and nanotubes may disrupt the polymer chain packing thus enhancing gas diffusion due to introducing more free volume voids between the polymer chains and nanoscaled defects on the polymer/nanofillers interface.

Tailoring free volume cavities by controlling the macromolecule's size and the structure of glassy polymer directly influences the gas transport properties.[24]. In particular, a class of high free volume, glassy, ladder type polymers, referred to as polymer of intrinsic microporosity (PIM) is a potential candidate for highly effective gas separation membranes comprising the capability for gas permeability and selectivity optimization by changing the polymer chain packing [25]. Budd and McKeown et al.[26, 27] were the first to report this new class of rigid ladder-type polydioxanes containing highly contorted chains. Among these, PIM-1, containing the contorted angled spirobisindane unit, has attracted the most attention due to its relative ease of synthesizing high molecular weight polymers and the combination of outstanding permeability with relatively moderate but technically attractive selectivity [28, 29], especially for O₂/N₂ and CO₂/CH₄ pairs, ranging among the upper bound trade-off introduced by Robeson [7].

In the present work, MMM were fabricated by loading of f-MWCNTs as an inorganic disperse phase into PIM-1 as a polymer matrix. MWCNTs were chosen because they had been proven to be promising nanofillers in tailoring polymeric material suited to be prescribed for application even at low incorporation [30]. To the best of our knowledge, so far there is no literature available on using MWCNTs combined with PIM-1 as polymer matrix for gas separation. However, it is well documented that for sufficient enhancement of MMM performance, the dispersion of MWCNTs in the polymer matrix should be very fine which means that the surface interaction between the filler and the polymer matrices should be strong [31]. In response to that, the MWCNTs were functionalized with poly(ethylene glycol) (PEG) as a spacer via "grafting to" method [32] to facilitate their dispersion in the PIM-1 matrix. The as prepared MMM were characterized for their morphology using scanning electron microscopy (SEM). Gas permeability and permselectivity were studied by pure gas permeation measurements.

2. Experimental :

2.1. Materials

The monomer 5,5',6,6'-tetrahydroxy-3,3,3',3'- tetramethyl-1,1'-spirobisindane (TTSBI, 97%) was obtained from ABCR, Germany and 2,3,5,6- tetrafluoroterephthalonitrile (TFTPN, 99%) was kindly donated by Lanxess (Germany). TFTPN was sublimated twice under vacuum prior to use. Potassium carbonate (K_2CO_3 , >99.5%) was dried overnight under vacuum at 120 °C in order to ensure no moisture is trapped in it and then milled in a ball mill for 15 min. MWCNTs were supplied by FutureCarbon GmbH (Germany) (purity >98%, surface area of 250 m²/g, diameter varies from 12 to 15 nm, and number of walls 8 to 12). SWCNTs were obtained from Fraunhofer-Institut für Werkstoff-und Strahltechnik IWS, Dresden (Germany) (diameter 1.1 to 1.4 nm, mean length of single SWCNT >10µm, purity >98%). Poly(ethylene glycol) of 200 g/mol and diethylbenzene (isomeric mixture) was purchased from Sigma-Aldrich, dimethyl acetamide (DMAc, ≥99%), nitric acid (HNO₃, 65% v/v), thionyl chloride (SOCl₂, ≥99%), tetrahydrofuran (THF≥99,9%), methanol (≥99.9%), chloroform (CHCl₃, 99.99%), dioxane (≥99%), from Merck were used as received.

2.2. Functionalization of MWCNTs

2.2.1. Oxidation of the MWCNTs

The MWCNTs were dispersed in HNO₃ in a round bottom flask. After 30 min of sonication at room temperature, the solution was heated to 65 °C and continuously stirred for 48 h. The solution was then filtered and washed with ample amounts of distilled water until neutrality (pH=7). Finally, the oxidized carbon nanotubes were dried under vacuum at 60 °C for 72 h.

2.2.2. Conversion of carboxylated MWCNTs to acyl chloride MWCNTs and esterification

The oxidized MWCNTs were chlorinated in presence of SOCl₂ for 24 h at 65 °C. After reaction, the dispersion was generously washed with THF, filtered, and dried overnight at ambient temperature. Then acyl chloride functionalized MWCNTs were added to PEG (200 g/mole) heated to 120 °C and stirred for 48 h. Finally functionalized carbon nanotubes were washed with THF and filtered through a Teflon[®] membrane (0.2 µm pore size), followed by drying at ambient temperature for 48 h [32].

2.3. Synthesis of polymer of intrinsic microporosity (PIM-1)

PIM-1 was prepared by using a fast synthesis method originally developed by Guiver *et al* [33]. A slightly modified procedure for PIM-1 [34-36] was carried out as follows: equimolar ratio of TTSBI, TFTPn dissolved in DMAc to form an orange-red solution. Addition of K_2CO_3 (2.3 times with respect to -OH monomer concentration) caused a colour change to yellow. The reaction mixture was immersed in an oil bath maintained at 150 °C and kept under a continuous flow of argon. After 5 min precipitate appeared and the reaction mixture became viscous, then diethylbenzene (DEB; same amount with respect to DMAc) was added into the reaction mixture, otherwise stirring could not be done easily. Stirring continued for one further hour and the polymer was isolated by precipitation in methanol and filtered off. The polymer was boiled in water for several hours to remove salts and solvent residues, and then filtered off and dried overnight at 60 °C. The dried polymer was dissolved in chloroform and re-precipitated again in methanol and then dried overnight at 60 °C under vacuum to give PIM-1 in 90 % yield. The weight averaged molecular weight (M_w) and molecular dispersity (M_w/M_n) of the prepared PIM-1 is 2.21×10^5 ($g\ mol^{-1}$) and 4.8, respectively, determined by size exclusion chromatography (SEC) in chloroform against polystyrene standards.

2.4. Mixed matrix membrane preparation

To prepare the film casting solution, the PIM-1 was first dissolved in chloroform and stirred for 2 h. Chloroform dispersions of f-MWCNTs were homogenized for 40 min with an ultrasonic probe (Bandelin SONOPULS, frequency = 20 kHz) and blended with PIM-1 polymer solution and stirred overnight. The blend ratio of f-MWCNTs was 0.5, 1, 2, 3wt % (in respect to polymer) with 2 wt% polymer concentration in casting solution. In a similar way, solutions of 1 wt% SWCNT and 1 wt% MWCNT with 2 wt% polymer concentration in casting solutions were prepared. The blended solution was poured into Teflon casting dish and evaporated under nitrogen atmosphere at room temperature, which has been covered to reduce evaporation rate. The average evaporation time for casting solutions were around 24 h. After solvent evaporation, the prepared films were delaminated and conditioned by soaking in methanol for approximately 4h. Immersing the membranes in methanol reverses prior film formation history, in a manner similar to protocols previously developed for microporous polyacetylenes and PIM-1 [37, 38]. The methanol treated membranes were dried in high vacuum for 16 h at 120 °C. The thickness of the membranes was measured by a digital micrometer (Deltascope[®] MP2C). The thickness and diameter of MMM before and after methanol treatment are given in Table 1.

2.5. Membrane characterization

2.5.1 Fourier transform infrared spectroscopy (FTIR)

Fourier transform infrared (FTIR) spectroscopy was conducted using a Bruker Equinox 55. The samples were mixed with KBr and pellets were prepared under hydraulic press force of 10 tons. Pellets were vacuum dried at 35 °C for 12 h. The transmission spectra were taken in a spectral range of 400-4000 cm⁻¹ with a resolution of 4 cm⁻¹ and average of 64 scans.

2.5.2. Thermal gravimetric analyses (TGA)

Thermal gravimetric analysis (TGA) was used to investigate the weight changes of f-MWCNTs samples and thermal properties of MMM as a function of temperature using Netzsch TG209 F1 Iris instrument. The experiments were conducted under argon flow from 25 °C to 900°C at 10° K/min. The weight loss was estimated from 100 °C to 800 °C in this study.

2.5.3. Scanning electron microscopy (SEM)

LEO 1550 VP instrument equipped with a field emission cathode operated at 1-1.5 kV was used to study the morphology of pure PIM-1 and MMM. SEM was also used to observe the compatibility between CNTs and the polymer matrix. For cross section analysis, the samples were fractured cryogenically in liquid nitrogen in order to have distinct view of membrane's selective layer section. Before scanning, the membrane samples were coated with Pt with a sputter-coater.

2.5.4. Gas Permeation measurement

Permeabilities of four pure gases (H₂, N₂, CO₂, CH₄) were measured by a pressure increase time-lag apparatus at 30 °C and permeability (*P*), diffusivity (*D*), solubility (*S*) and selectivity (α) for gases A and B were determined under steady state by the following equations :

$$P = DS = \frac{V_p l (p_{p2} - p_{p1})}{ART\Delta t (p_f - (p_{p2} + p_{p1})/2)} \quad (1)$$

$$D = \frac{l^2}{6\theta} \quad (2)$$

$$\alpha_{A/B} = \frac{P_A}{P_B} = \frac{D_A S_A}{D_B S_B} \quad (3)$$

where V_p is the constant permeate volume, R is the gas constant, l is the film thickness, A is the effective area of membrane, Δt is the time for permeate pressure increase from p_{p1} to p_{p2} , p_f is the feed pressure, and θ is called time-lag [39]. The solution–diffusion transport model [40] was applied for discussing the gas transport properties of dense polymer f-MWCNT/PIM-1 membranes, and the selectivities of membranes for gas “A” relative to another gas “B” which is the ratio of their permeabilities obtained from Eq. (3).

2.5.5. Gravimetric adsorption balance:

Adsorption measurements of the pure gases were performed on a magnetic suspension balance, Rubotherm (Bochum, Germany). For each measurement samples were degassed at 353 K for 18 h at $P \leq 10^{-6}$ mbar. All tubing and chambers were also degassed by applying vacuum ($P \leq 10^{-6}$ mbar). The degassed samples were then cooled down to the specified temperature (303 K) with the ramping rate of 1 K/min. The gases with a purity of 99.99% were used in this measurement. The gravimetric sorption studies in this research were conducted at a temperature of 303 ± 0.1 K and a pressure range of 0.01- 8 bar.

2.5.6. Mechanical analysis

Measurements of tensile mechanical properties of the prepared MMM were performed on a Zwick Z020 with a load cell of 1kN. Stripes of the membranes with 3 cm effective length and 1 cm width were measured at crosshead speed of 2 mm/min. The values of Young’s modulus, tensile strength and elongation at break were determined. At least five specimens were tested for each sample and the average values, together with the standard deviations, are reported.

3. Results and discussion

3.1. Functionalization of MWCNTs

The surface modification of MWCNTs followed by covalent bonding of polymer chains on the surface of MWCNTs is depicted in Scheme 1. A similar procedure has been reported previously by other groups [41, 42]. The first step shows the oxidation of pristine MWCNTs with HNO_3 . The aim of the chosen acid treatment is disaggregation of nanotube bundles, dissolution of the catalysts and the synthesis by-products (e.g., amorphous carbon). Further reaction between the oxidized carbon nanotubes and thionyl chloride leads to the formation of acyl chloride groups. The acyl chloride groups are highly reactive and can further react with poly(ethylene glycol) to form esters.

3.2. Characterization of *f*-MWCNTs and *f*-MWCNTs/PIM-1 MMM

Fig. 1 shows the infrared spectrum of the pristine MWCNTs and PEG grafted MWCNTs. The signals between 1650 cm^{-1} and 1540 cm^{-1} indicate the C=C stretching mode of the aromatic ring. The peak at 1724 cm^{-1} is attributed to the C=O stretching vibration of the ester carbonyl group. The stretching vibrations of the repeated $-\text{OCH}_2\text{CH}_2$ units of PEG and $-\text{COO}-$ bonds were observed at 1092 cm^{-1} and 1240 cm^{-1} , respectively, which is the evidence for successful reaction. An asymmetric and symmetric stretching of C-H deformation is observed for PEG-MWCNTs at 2927 cm^{-1} and 2853 cm^{-1} , respectively, which is not observed in MWCNTs spectra but clearly observed in PEG-MWCNTs. TGA of pristine and *f*-MWCNTs is not shown here but the amount of PEG chains grafted on the MWCNTs was estimated based on these results and the concentration of PEG chains on the MWCNTs were calculated to be about 0.09 mmol/g . The thermal properties of *f*-MWCNTs/PIM-1 MMM were characterized also by TGA (Fig. 2). The onset decomposition temperature of the samples was observed at about $503\pm 1\text{ }^\circ\text{C}$, as shown in Fig.2. Because of the lack of rotational mobility in the backbone of the rigid ladder polymer, it is difficult to observe a glass transition temperature before degradation [43].

3.3. Polymer (PIM-1) synthesis

PIM-1 was synthesized by reacting molar equivalents of 5,5',6,6'-tetrahydroxy-3,3',3',3'-tetramethyl-1,1'-spirobisindane (TTSBI) and 2,3,5,6- tetrafluoroterephthalonitrile (TFTPN) with an excess of K_2CO_3 (Scheme 2). The polymer was synthesized based on the modified rapid synthesis of PIM-1. Different from previous polymerization protocols [33], diethylbenzene (DEB) was introduced to this reaction system instead of toluene, seemingly advantageous because of its higher boiling point ($150\text{ }^\circ\text{C}$) [44]. DEB was added in the required minimal amounts to keep the viscosity sufficiently low. The polymer was characterized by ^1H NMR and IR spectroscopy.

3.4. MMM morphology

3.4.1. Effect of pristine SWCNTs, MWCNTs and *f*-MWCNTs on MMM morphology

Fig. 3 shows the cross section and surface (inset) SEM images of the prepared membrane. Fig.3 (a) shows the cross section and in inset shows the smooth surface of the pure PIM-1 membrane which was nearly defect free. The cross section images of *f*-MWCNTs, pristine SWCNTs and MWCNTs MMM depict a noticeable difference. Functionalized MWCNTs

were well dispersed in the PIM-1 matrix [shown by the white circle Fig.3 (b)]. When pristine SWCNTs (Fig. 3d) and MWCNTs (Fig. 3c) were incorporated into the PIM-1 matrix, the resulting MMM contained agglomerated CNTs which are clearly observable from the cross section [shown by white circle in Fig.3(c-d)]. The explanation for agglomeration of pristine SWCNTs and MWCNTs in the polymer matrix was that the interactions among pristine MWCNTs and SWCNTs (π - π interaction) are stronger than those with the polymer matrix [45, 46]. Therefore pristine SWCNTs and MWCNTs tend to agglomerate, do not distribute well and form a micron level sponge structure within PIM-1 matrix. Functionalization on the surface of MWCNTs appeared to de-bundle the highly entangled MWCNTs which resulted in improved dispersion throughout the PIM-1 matrix. From these cross-section morphologies we can conclude that the incorporation of f-MWCNTs in polymer matrix led to better dispersion than pristine SWCNTs and MWCNTs.

3.4.2. Effect of f-MWCNT content on MMM morphology

Fig. 4 shows the morphology of PIM-1/f-MWCNTs MMM at different f-MWCNTs loading. Figs.4a-c (surface) & 4e-g (cross section) depict the f-MWCNTs tend to be well distributed throughout the polymer matrix independent of the f-MWCNT loading (0.5 to 2 wt %). No evidence of f-MWCNT agglomeration or interface void was found even at higher magnification. As the MWCNTs loadings were further increased from 2 to 3 wt%, the nanotubes tend to agglomerate and to be not well distributed throughout the PIM-1 matrix. Also the defects and interface voids around the f-MWCNTs agglomerates observed on the surface of this MMM [Fig.4 (d, h)]. Therefore more interface voids and agglomeration decreased the permeability of gases as the f-MWCNTs loading in PIM-1 matrix were increased from 2 to 3 wt%.

From these observations, we conclude that the threshold limit for the addition of CNTs to the polymer matrix to prevent agglomeration is typically around 3 wt% and the optimum for the addition of f-MWCNTs is 2 wt%.

3.5. Gas permeation measurement

3.5.1. Effects of pristine SWCNTs, MWCNTs and f-MWCNTs on MMM gas separation performance

The gas permeation properties of MMM were investigated by incorporating 1 wt% of pristine SWCNTs, pristine MWCNTs and PEG functionalized MWCNT in PIM-1 matrix.

Permeability of CO₂, CH₄, N₂, and O₂ and various gas pair selectivity for pure PIM-1 and MMM are shown in Table 2.

The highest permeability of the gases was found for 1 wt % pristine SWCNTs/PIM MMM. The increase of CO₂ permeability after incorporation of 1 wt % pristine SWCNTs was 153%, although slight loss of selectivity (25%) was observed which is very promising for applications where high permeability with moderate selectivity is required.

Permeation measurements were carried out using pure O₂, N₂, CO₂, CH₄ at 2 bar feed pressure at 30 °C. It was observed that the MMM incorporated with pristine SWCNTs, MWCNTs and PEG functionalized MWCNTs have higher gas permeabilities compared to pure PIM-1. The selectivities of CO₂/N₂ and CO₂/CH₄ decreased with pristine SWCNTs, MWCNTs and f-MWCNTs addition. Despite increase in permeability of O₂ and N₂, the O₂/N₂ separation factor remains unchanged because CNTs are not selective for either O₂ or N₂. Few researchers [47-49] have investigated the physical adsorption of gas in CNTs and they found that the inner hollow cavities of CNTs could hold molecules or atoms by adsorption or capillarity while Yang et al.[50] reported that the aggregated pores of high purity MWCNTs can adsorb N₂ gas as extremely high as 750 mg/g.

3.5.2. Effects of f-MWCNTs content on MMM gas separation performance

In order to investigate systematically the effect of f-MWCNTs incorporation on the MMM gas separation performance, MMM were fabricated with different loadings of f-MWCNT. The permeability of He, O₂, N₂, CO₂, CH₄ at different f-MWCNTs loadings are shown in Table 3. The order of gas permeability was observed as CO₂ > He > O₂ > CH₄ > N₂. The addition of 0.5wt% of f-MWCNTs loading to polymer matrix resulted in ~ 12% increase in permeability of He and N₂, while permeability of O₂, CO₂ and CH₄ increased ~ 7%, 21% and 74%, respectively. Furthermore, significant enhancement in permeability as a function of f-MWCNTs loading in the polymer matrix was observed between 1 wt% to 2 wt%. An increase in free volume of the PIM-1 as a result of the disruption of the polymer chains packing due to the interaction between the surface of PEG functionalized MWCNTs and the PIM-1 chains might have contributed to the increment of the permeability. The permeability for gas molecules such as He, N₂, O₂, CO₂ and CH₄ decreased as f-MWCNTs loading in polymer matrix increased from 2 wt% to 3 wt%. From the SEM images, one can see that the f-MWCNTs are well dispersed in the polymer matrix at 0.5 wt% to 2wt% loading [Fig.4 (e-g)]. In these cases MMM can perform higher gas permeability because the well dispersed f-MWCNTs would serve as channels to transport gas molecule more effectively. From the

previous report about permeation enhancement of MMM [14, 20-22], the results suggest that the interaction between polymer-chain segments and CNTs may disrupt the polymer-chain packing and thus enhance the gas diffusion due to more free volume introduced among the polymer chains and defects at polymer/nanofillers interface. Some agglomerates and clusters of nanotubes form in the polymer matrix at high loading ratio (3 wt %), that may decrease the total free volume and tortuosity around the agglomerated f-MWCNTs domains leading to a slight deterioration of the permeation.

In addition, the gas permeabilities of PIM-1 containing f-MWCNTs are higher than those of pure PIM-1 and increasing up to the optimum. This trend is more clearly shown in Fig.5, which presents the relative permeability of PIM-1 f-MWCNTs MMM to O₂, N₂, CH₄, and CO₂ as a function of the f-MWCNTs content. For all penetrant gases, the permeability of PIM-1 containing f-MWCNTs is higher than that of pure PIM-1 and also increases with increasing f-MWCNTs content from 0.5 wt% to 2 wt%.

The solution-diffusion model was applied to investigate many dense polymer membranes separation processes [40]. Based on this model, the penetrant dissolves in the membrane materials and then diffuses through the membrane following the concentration gradient. In this study, performed by time-lag method, the difference in permeabilities of each MMM can be better understood by analyzing the contribution of diffusivity and solubility coefficient to the overall permeabilities. The diffusion coefficients calculated by Eq. 2 are shown in Table 4. The diffusion coefficients are not reported here because the diffusion of He is too fast for the time-lag method. After loading of 0.5 wt% f-MWCNTs to the polymer matrix, diffusion coefficients for N₂, O₂, CO₂ increased by around 15-20% and by ~2% for CH₄. At 1 wt% to 2 wt% f-MWCNTs loading in the polymer matrix, the diffusivities of all gases increased further, for example up to 145% for CO₂. It can be assumed that the interface between CNTs and polymer chains are continuous at lower CNTs loading (0.5-2 wt%) leading to lower gas diffusion resistance. However, at 3 wt% f-MWCNTs loading the diffusivities for all gases are lower than those observed at 2 wt% f-MWCNTs and it may be possible that the created nano-gaps between CNTs and polymer chain become discontinuous. To show this more clearly, the relative diffusivity of f-MWCNT/PIM-1 MMM for different gases is shown in Fig.6. Moreover the solubility coefficients calculated from time-lag method for N₂, O₂, CO₂, and CH₄ shown in Fig.7. Despite increase in permeability and diffusivity, the N₂, O₂, and CH₄ solubility does not show any big difference after the f-MWCNTs addition into the polymer matrix, while the CO₂ gas solubility increases gradually at loadings 0.5 wt% to 3 wt%. From the previous studies it is well known that, ethylene oxide units provide good solubility of

condensable CO₂ gas in the polymer membrane due to affinity of the polar ether oxygen and quadrupolar gas CO₂ [51].

These observations indicate that at f-MWCNTs loadings higher than 2 wt%, permeability and diffusivity of the N₂, O₂, CO₂, and CH₄ gases show a significant drop (shown in Fig.5 & 6).

Table 5 shows the selectivity of various gas pairs of PIM-1 and f-MWCNTs MMMs. At 0.5 wt% to 2 wt% f-MWCNTs loading the selectivity of O₂/N₂, CO₂/CH₄ and He/CH₄ was found to be decreased compared to the pure PIM-1. But the selectivity increased at 3 wt% f-MWCNTs loading due to significant decrease in permeability. The high selectivity values of CO₂/N₂ at 0.5 wt% f-MWCNTs loading might have resulted due to the intimate interface interaction of f-MWCNTs-polymer chain. Despite increase in permeability of O₂ and N₂, the O₂/N₂ separation factor did not show a big change and this might indicate that f-MWCNTs are not selective for either O₂ or N₂. In addition, the observed decrease in He/CH₄ selectivity agrees well with the selectivity and flux for CH₄/H₂ separation calculated by atomistic simulation by Chen and Sholl [52]. Again from Table 3, which shows an increase in CH₄ permeability by ~75%, while He permeability increased by 11% at 0.5 wt% f-MWCNTs loading. Hence the separation factors for He/CH₄ and CO₂/CH₄ decreased with the addition of f-MWCNTs due to preferential sorption of CH₄ in the f-MWCNTs. Despite increase in permeability of O₂ and N₂, the O₂/N₂ separation factor did not show any big change because f-MWCNTs are not selective for either O₂ or N₂. In addition, a small change in the O₂/N₂ separation factor of MMMs suggests that the prepared membranes do not have any nonselective voids at the f-MWCNTs/PIM-1 interface.

Fig. 8 (a-b) represents N₂, CO₂ sorption isotherm in PIM-1 and PIM-1 containing 0.5, 1, 2 and 3 wt% functionalized MWCNTs at 303 K. The specific uptake (m_{ADS}) in MMM for N₂ and CO₂ depends on the f-MWCNTs content. However, the specific uptake is lower in the MMM with 3 wt% of f-MWCNTs in comparison to the increase seen at the MMMs with 0.5, 1 and 2 wt% of f-MWCNTs. From the mechanical testing data, it has been implied that the interaction between the f-MWCNTs and the polymer chain can create an interfacial zone with reoriented polymer chain with different mobility[53]. These results suggest that the presence of f-MWCNTs increases the specific uptake (relative sorption) of gases in the MMM at higher f-MWCNTs content, and beyond the optimum the decrement may be countered by constrained polymer chain packing at f-MWCNTs/polymer interface.

The gas separation performance of the f-MWCNTs/PIM MMM was plotted on the Robeson's upper bound plot [7] in order to compare the results with the literature data. Fig.9 shows the Robeson's upper bound 2008 for CO₂/N₂ gas pairs and the position of the data points for the

PIM-1 and f-MWCNTs/PIM-1 system with different f-MWCNTs content. Incorporation of f-MWCNTs in PIM-1 polymer increases the efficiency of this membrane type in the separation of CO₂ gas respect to N₂.

3.5.3. Influence of temperature on gas separation performance of f-MWCNTs MMM:

Temperature effects on membrane performance were studied over a temperature range of 283-333 K (single gas at 1 bar feed pressure). Fig.10 shows the permeability of N₂, CH₄, CO₂, and O₂ for PIM-1 and PIM-1/f-MWCNT MMM as a function of the inverse absolute temperature. Fig.10 shows that permeability of the N₂ and CH₄ increased with increasing in temperature while for CO₂ and O₂, the permeability decreased with increasing temperature. This indicates that the effect of highly sorbed gases like CO₂ does not affect the permeation rate of lighter gases in subsequent runs [54]. But a careful examination reveals that the permeability of all gases is higher in 0.5 to 2 wt% f-MWCNTs-PIM-1 MMMs than in the sample with 3 wt% f-MWCNTs and the pure polymeric membrane at all temperature. Fig.11 shows the O₂/N₂, CO₂/N₂, and CO₂/CH₄ selectivity of the pure PIM-1 and f-MWCNTs PIM-1 MMMs as a function of inverse absolute temperature. It is observed that the selectivity for a given gas pair decreases with an increase in temperature of pure PIM-1 and f-MWCNTs PIM-1 MMMs. Hence, incorporation of f-MWCNTs did not change any selectivity pattern at higher temperature. However, a significant difference in selectivity at lower temperature was observed for PIM-1. It shows, O₂/N₂ selectivity at 333 K is nearly 2.7; at 283 K it reaches 4.6 while for CO₂/N₂ selectivity is around 30.9 at low temperature and 14.1 at elevated temperature 333K.

In order to explore the temperature dependence of N₂, O₂, CO₂, CH₄ permeabilities in these membranes, resulting data were correlated with the Arrhenius equation. Thus, the activation energy of permeation (E_p) was determined by the Arrhenius relationship:

$$P = P_o \exp\left(\frac{-E_p}{RT}\right) \quad (4)$$

P is permeability, P_o is a pre-exponential factor, E_p is the activation energy of permeation (J/mole), R is the gas constant (8.314 J/(mol K)) and T is the absolute temperature. The given equation is valid in a temperature range which does not cause significant thermal transitions in the polymer.

The activation energy of permeation (E_p), determined from the slope of the Arrhenius plot is shown in Table 6. It provides a qualitative measure of free volume and the size of molecular

gaps between chain segments. The activation energy of permeation is the sum of the activation energy of diffusion, E_d , and the enthalpy of sorption, ΔH_s ,

$$E_p = E_d + \Delta H_s \quad (5)$$

In essentially all conventional glassy polymers, gas permeability increases with increased temperature, because $E_d + H_s > 0$ and $|E_d| / |H_s| > 1$. An exception to this rule is the temperature dependence of gas permeability in high-free-volume PIM-1 [54], i.e. gas permeabilities decrease with increased temperature for condensable gases like CO₂ ($|E_d| / |H_s| < 1$). Therefore, negative activation energies of permeation in PIM-1 result from very small activation energies of diffusion, which indicates that the dependence of permeability on temperature is much weaker. Also the negative value of E_p is the characteristics for the decrease of permeability with the increase of temperature which is observed in Fig. 10 (CO₂ permeability). On the other hand CH₄ and N₂ permeability of PIM-1 depend strongly on temperature and their E_p values are essentially of the same order of magnitude as those of conventional glassy polymers. The activation energies of permeation in 0.5 wt% MMM are only slightly higher than those of pure PIM-1, then significantly lower for further addition of f-MWCNTs to the polymer matrix, as shown in Table.6. The highest decrease of E_p observed for all gases in 2 wt% MMM. Furthermore, negative activation energies of permeation are routinely observed for microporous solids in which the pore dimensions are relatively large in comparison with the diffusing gas molecules. It is reasonable, therefore, to suggest that the ultra high free- volume glassy polymers resemble microporous solids and comprise a network of interconnected gaps with dimensions large compared to the diffusing gas molecules [55].

3.5.4. Influence of pressure on gas separation performance of f-MWCNTs MMM:

The permeabilities of f-MWCNT/PIM-1 MMM were determined as a function of the feed pressure. The measurements were carried out with N₂, CO₂, and CH₄ at 25 C and pressures up to 30 atm [Fig.12 (a-c)]. In typical glassy polymers, the permeability decreases with increasing pressure due to the filling of Langmuir sorption sites, while at higher pressure, the contribution of the Langmuir region to the overall permeability diminishes and gas permeability approaches a constant value associated with simple dissolution (Henry's law) transport [56]. Fig.12 shows that the permeability decreased with increasing the feed pressure from 5 to 30 bar. It indicates absence of plasticization in the MMMs. However, in the presence of plasticization especially for CO₂ the membranes show high permeability values after achieving the lowest values at higher pressures, which indicates swelling of membranes.

Moreover, the f-MWCNT/PIM-1 MMM show the higher permeability compared to one prepared from pure polymer (except 3 wt% f-MWCNT/PIM-1 MMM) at different feed pressures. In comparison with 1 wt% and 2 wt% f-MWCNT/PIM-1 MMM, the N_2 , CO_2 , CH_4 permeabilities of PIM-1 declined by around 40% at 25 atm and permeability decline of 1 wt% and 2 wt% f-MWCNT/PIM-1 MMM at high pressure was less. A significant loss in gas permeability shows that the microporous structure of the polymer is affected at high pressure.

3.6. Mechanical properties

Carbon nanotubes have an extremely high tensile modulus (50-1000GPa)[45, 57], tensile strength (20-150 GPa)[46, 58], and high aspect ratio (typically ~300-1000)[51]. The addition of small amounts of CNTs to a polymer matrix is expected to enhance the mechanical properties significantly[53, 59]. The summary of mechanical properties obtained from the films of PIM-1 and f-MWCNTs /PIM-1 MMM, in terms of Young's modulus (E), tensile strength (σ_M), and elongation at break (ϵ) with standard deviations is reported in Table 7. The Young's modulus and tensile strength improve linearly with the maximum enhancement of 29% and 23% in 2 wt% f-MWCNTs/PIM-1 MMM, respectively, in comparison with pure PIM-1. Likewise, the maximum of the elongation at break also was found at 2 wt% f-MWCNTs loading. However, a decrease in these properties was observed at 3 wt% f-MWCNTs loading. The noticeable increase in Young's modulus and tensile strength from 0 to 2 wt% f-MWCNTs loading thus can be attributed to the better dispersion of f-MWCNTs and better interfacial interaction between the functionalized MWCNTs and polymer matrix [evident from Fig.4 (e, f, g)]. However, a decrease in mechanical properties at 3 wt% f-MWCNTs loading can be attributed to strong attractive forces between f-MWCNTs leading to excessive agglomeration [evident from Fig.4 (h)]. So the overall mechanical properties were improved for samples with lower loadings of f-MWCNTs as long as they dispersed in the matrix properly.

4. Conclusion

Mixed matrix membranes were successfully prepared by dispersing MWCNTs (pristine and functionalized) into the PIM-1 polymer matrix. The functionalized MWCNTs were obtained via 'grafting to' method and characterized by FTIR and TGA. The f-MWCNTs dispersed better than pristine MWCNTs, in the polymer matrix as well as in chloroform. The cross-sectional SEM images of MMM films indicated that the f-MWCNTs were well dispersed in the polymer matrix at loadings of 0.5 wt% to 2 wt% f-MWCNTs, while at 3 wt% the

nanotubes agglomerated and formed domains or interface voids in the polymer matrix. The gas permeation fluxes of the derived membranes are increased with nanotubes loading of 0.5-2 wt% without sacrificing selectivity. The gas transport in the f-MWCNTs/PIM-1 MMM through the free volume of the polymer chains or MWCNTs channels increases the gas diffusivity and results in a higher permeation. The f-MWCNTs/PIM-1 MMM shows only a weak dependence of gas permeability on temperature. The activation energies of permeation of f-MWCNTs/PIM-1 MMM were lower than pure PIM-1 (except 0.5 wt%) and permeability was decreasing with increased temperature. Moreover, the permeability of f-MWCNTs/PIM-1 MMM decreased with increase in feed pressure, indicating no plasticization. Improvements of tensile strength, Young's modulus and elongation at break with concentration of f-MWCNTs (2 wt%) of f-MWCNTs/PIM-1 MMM were obtained. The strong interaction between the f-MWCNTs and the PIM-1 matrix greatly enhanced the interfacial adhesion, thus strengthening the overall mechanical performance of the MMM.

Acknowledgements

The authors would like to thank Silke Dargel, Silvio Neumann, Heinrich Böttcher, Bahadir N. Gacal, Shahid Majeed, and Anne Schroeder for their technical support, and Oliver Jost from the IWS for supplying the SWCNT. This work was financially supported by the project 'High Aspect Ratio Carbon-based Nanocomposites' (HARCANA) within the European Community's 7th Framework Programme for Research and Technological Development under the grant agreement number NMP3-LA-2008-213277. This work also benefited from the Project 'CarboFunk' (BMBF F.kennz. 03X0041) within the Inno.CNT program funded by the German Bundesministerium für Bildung und Forschung and the Helmholtz Association of German Research Centres through the Helmholtz Portfolio MEM-BRAIN.

5. References

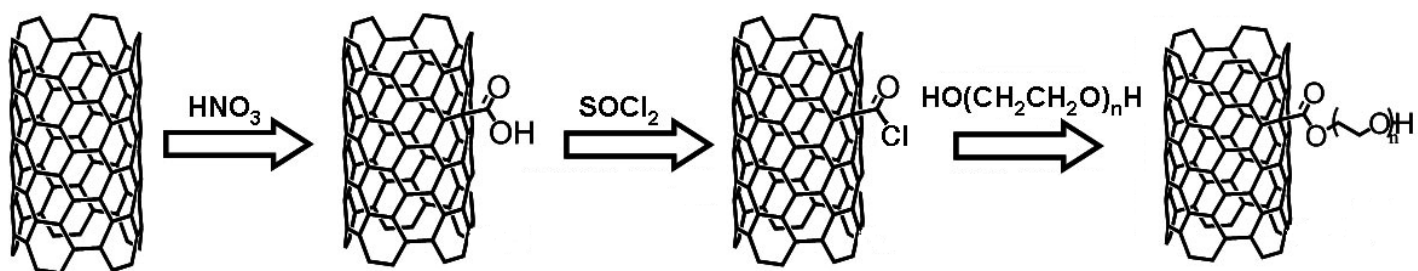
- [1] W.J.Koros, Gas separation membranes: needs for combined materials science and processing approaches, *Macromol. Symp*, 188 (2002) 13-22.
- [2] P. Pandey, R.S. Chauhan, Membranes for gas separation, *Progress in Polymer Science*, 26 (2001) 853-893.
- [3] G. Maier, Gas Separation with Polymer Membranes, *Angewandte Chemie International Edition*, 37 (1998) 2960-2974.
- [4] A.F. Ismail, W. Lorna, Penetrant-induced plasticization phenomenon in glassy polymers for gas separation membrane, *Separation and Purification Technology*, 27 (2002) 173-194.
- [5] S.C. George, S. Thomas, Transport phenomena through polymeric systems, *Progress in Polymer Science*, 26 (2001) 985-1017.

- [6] B.D. Freeman, I.Pinnau, Polymeric materials for gas separations, ACS Symp. Ser, 733 (1999) 1-27.
- [7] L.M. Robeson, The upper bound revisited, Journal of Membrane Science, 320 (2008) 390-400.
- [8] F. Peng, L. Lu, H. Sun, Y. Wang, J. Liu, Z. Jiang, Hybrid Organic–Inorganic Membrane: Solving the Tradeoff between Permeability and Selectivity, Chemistry of Materials, 17 (2005) 6790-6796.
- [9] J. Kim, B. Van der Bruggen, The use of nanoparticles in polymeric and ceramic membrane structures: Review of manufacturing procedures and performance improvement for water treatment, Environmental Pollution, 158 (2010) 2335-2349.
- [10] Y. Li, T.-S. Chung, C. Cao, S. Kulprathipanja, The effects of polymer chain rigidification, zeolite pore size and pore blockage on polyethersulfone (PES)-zeolite A mixed matrix membranes, Journal of Membrane Science, 260 (2005) 45-55.
- [11] C. Joly, M. Smaïhi, L. Porcar, R.D. Noble, Polyimide–Silica Composite Materials: How Does Silica Influence Their Microstructure and Gas Permeation Properties?, Chemistry of Materials, 11 (1999) 2331-2338.
- [12] C. Joly, S. Goizet, J.C. Schrotter, J. Sanchez, M. Escoubes, Sol-gel polyimide-silica composite membrane: gas transport properties, Journal of Membrane Science, 130 (1997) 63-74.
- [13] A.F. Ismail, R.A. Rahim, W.A.W.A. Rahman, Characterization of polyethersulfone/Matrimid[®] 5218 miscible blend mixed matrix membranes for O₂/N₂ gas separation, Separation and Purification Technology, 63 (2008) 200-206.
- [14] Q. Hu, E. Marand, S. Dhingra, D. Fritsch, J. Wen, G. Wilkes, Poly(amide-imide)/TiO₂ nano-composite gas separation membranes: Fabrication and characterization, Journal of Membrane Science, 135 (1997) 65-79.
- [15] L. Song, H. Zhang, Z. Zhang, S. Xie, Processing and performance improvements of SWNT paper reinforced PEEK nanocomposites, Composites Part A: Applied Science and Manufacturing, 38 (2007) 388-392.
- [16] D. Qian, E.C. Dickey, R. Andrews, T. Rantell, Load transfer and deformation mechanisms in carbon nanotube-polystyrene composites, Applied Physics Letters, 76 (2000) 2868-2870.
- [17] T. Gong, Y. Zhang, W. Liu, J. Wei, Y. Jia, K. Wang, D. Wu, M. Zhong, Reinforcing the bandaged joint of double-walled carbon nanotube strands by intercalation of epoxy resin, Materials Letters, 62 (2008) 4431-4433.
- [18] A.I. Skoulidas, D.M. Ackerman, J.K. Johnson, D.S. Sholl, Rapid Transport of Gases in Carbon Nanotubes, Physical Review Letters, 89 (2002) 185901.
- [19] D.M. Ackerman, A.I. Skoulidas, D.S. Sholl, J. Karl Johnson, Diffusivities of Ar and Ne in Carbon Nanotubes, Molecular Simulation, 29 (2003) 677-684.
- [20] S. Kim, T.W. Pechar, E. Marand, Poly(imide siloxane) and carbon nanotube mixed matrix membranes for gas separation, Desalination, 192 (2006) 330-339.
- [21] H. Cong, J. Zhang, M. Radosz, Y. Shen, Carbon nanotube composite membranes of brominated poly(2,6-diphenyl-1,4-phenylene oxide) for gas separation, Journal of Membrane Science, 294 (2007) 178-185.
- [22] T.-H. Weng, H.-H. Tseng, M.-Y. Wey, Preparation and characterization of multi-walled carbon nanotube/PBNPI nanocomposite membrane for H₂/CH₄ separation, International Journal of Hydrogen Energy, 34 (2009) 8707-8715.
- [23] I. Pinnau, Z. He, Filled super glassy membrane, U.S. Patent, 6 (2001) 684.
- [24] H.B. Park, C.H. Jung, Y.M. Lee, A.J. Hill, S.J. Pas, S.T. Mudie, E. Van Wagner, B.D. Freeman, D.J. Cookson, Polymers with Cavities Tuned for Fast Selective Transport of Small Molecules and Ions, Science, 318 (2007) 254-258.

- [25] C.M. Zimmerman, W.J. Koros, Polypyrrolones for membrane gas separations. I. Structural comparison of gas transport and sorption properties, *Journal of Polymer Science Part B: Polymer Physics*, 37 (1999) 1235-1249.
- [26] N.B. McKeown, P.M. Budd, Msayib K, Ghanem, B., Microporous polymer material, International patent, WO05012397 (2005).
- [27] N.B. McKeown, Makhseed S., Organic microporous materials, International patent, WO03000774 (2003).
- [28] N.B. McKeown, P.M. Budd, Polymers of intrinsic microporosity (PIMs): organic materials for membrane separations, heterogeneous catalysis and hydrogen storage, *Chemical Society Reviews*, 35 (2006) 675-683.
- [29] N.B. McKeown, P.M. Budd, Msayib K, Ghanem, B., Microporous polymer material, US Patent Appl, 20060246273 (2006).
- [30] D. Bikiaris, A. Vassiliou, K. Chrissafis, K.M. Paraskevopoulos, A. Jannakoudakis, A. Docoslis, Effect of acid treated multi-walled carbon nanotubes on the mechanical, permeability, thermal properties and thermo-oxidative stability of isotactic polypropylene, *Polymer Degradation and Stability*, 93 (2008) 952-967.
- [31] T.-S. Chung, L.Y. Jiang, Y. Li, S. Kulprathipanja, Mixed matrix membranes (MMMs) comprising organic polymers with dispersed inorganic fillers for gas separation, *Progress in Polymer Science*, 32 (2007) 483-507.
- [32] J. Albuerno, A. Boschetti-de-Fierro, V. Abetz, Modification of multiwall carbon nanotubes by grafting from controlled polymerization of styrene: Effect of the characteristics of the nanotubes, *Journal of Polymer Science Part B: Polymer Physics*, 48 (2010) 1035-1046.
- [33] N. Du, J. Song, G.P. Robertson, I. Pinnau, M.D. Guiver, Linear High Molecular Weight Ladder Polymer via Fast Polycondensation of 5,5',6,6'-Tetrahydroxy-3,3,3',3'-tetramethylspirobisindane with 1,4-Dicyanotetrafluorobenzene, *Macromolecular Rapid Communications*, 29 (2008) 783-788.
- [34] D. Fritsch, G. Bengtson, M. Carta, N.B. McKeown, Synthesis and Gas Permeation Properties of Spirobischromane-Based Polymers of Intrinsic Microporosity, *Macromolecular Chemistry and Physics*, 212 (2011) 1137-1146.
- [35] M.M. Khan, V. Filiz, G. Bengtson, S. Shishatskiy, M.M. Rahman, V. Abetz, Functionalized carbon nanotubes mixed matrix membranes of polymers of intrinsic microporosity for gas separation, *Nanoscale Research Letters*, 7 (2012) 504.
- [36] M.M. Khan, V. Filiz, G. Bengtson, M.M. Rahman, S. Shishatskiy, V. Abetz, Functionalized Carbon Nanotube Mixed Matrix Membranes of Polymers of Intrinsic Microporosity (PIMs) for Gas Separation, *Procedia Engineering*, 44 (2012) 1899-1901.
- [37] K. Nagai, L.G. Toy, B.D. Freeman, M. Teraguchi, T. Masuda, I. Pinnau, Gas permeability and hydrocarbon solubility of poly[1-phenyl-2-[p-(triisopropylsilyl)phenyl]acetylene], *Journal of Polymer Science Part B: Polymer Physics*, 38 (2000) 1474-1484.
- [38] A.J. Hill, S.J. Pas, T.J. Bastow, M.I. Bugar, K. Nagai, L.G. Toy, B.D. Freeman, Influence of methanol conditioning and physical aging on carbon spin-lattice relaxation times of poly(1-trimethylsilyl-1-propyne), *Journal of Membrane Science*, 243 (2004) 37-44.
- [39] A.M. Shishatskii, Y.P. Yampol'skii, K.V. Peinemann, Effects of film thickness on density and gas permeation parameters of glassy polymers, *Journal of Membrane Science*, 112 (1996) 275-285.
- [40] J.G. Wijmans, R.W. Baker, The solution-diffusion model: a review, *Journal of Membrane Science*, 107 (1995) 1-21.
- [41] S. Qin, D. Qin, W.T. Ford, D.E. Resasco, J.E. Herrera, Functionalization of Single-Walled Carbon Nanotubes with Polystyrene via Grafting to and Grafting from Methods, *Macromolecules*, 37 (2004) 752-757.

- [42] H. Kong, C. Gao, D. Yan, Functionalization of Multiwalled Carbon Nanotubes by Atom Transfer Radical Polymerization and Defunctionalization of the Products, *Macromolecules*, 37 (2004) 4022-4030.
- [43] P.M. Budd, K.J. Msayib, C.E. Tattershall, B.S. Ghanem, K.J. Reynolds, N.B. McKeown, D. Fritsch, Gas separation membranes from polymers of intrinsic microporosity, *Journal of Membrane Science*, 251 (2005) 263-269.
- [44] D. Fritsch, K. Heinrich, G. Bengtson, *PMSE Prepr*, 101 (2009) 761.
- [45] W. Jeong, M.R. Kessler, Toughness Enhancement in ROMP Functionalized Carbon Nanotube/Polydicyclopentadiene Composites, *Chemistry of Materials*, 20 (2008) 7060-7068.
- [46] K. Stano, K. Koziol, M. Pick, M. Motta, A. Moisala, J. Vilatela, S. Frasier, A. Windle, Direct spinning of carbon nanotube fibres from liquid feedstock, *International Journal of Material Forming*, 1 (2008) 59-62.
- [47] Y.F. Yin, T. Mays, B. McEnaney, Adsorption of Nitrogen in Carbon Nanotube Arrays, *Langmuir*, 15 (1999) 8714-8718.
- [48] D. Ugarte, A. Châtelain, W.A. de Heer, Nanocapillarity and Chemistry in Carbon Nanotubes, *Science*, 274 (1996) 1897-1899.
- [49] E. Dujardin, T.W. Ebbesen, H. Hiura, K. Tanigaki, Capillarity and Wetting of Carbon Nanotubes, *Science*, 265 (1994) 1850-1852.
- [50] J. Yang, Y. Lin, J. Wang, M. Lai, J. Li, J. Liu, X. Tong, H. Cheng, Morphology, thermal stability, and dynamic mechanical properties of atactic polypropylene/carbon nanotube composites, *Journal of Applied Polymer Science*, 98 (2005) 1087-1091.
- [51] S. Xie, W. Li, Z. Pan, B. Chang, L. Sun, Mechanical and physical properties on carbon nanotube, *Journal of Physics and Chemistry of Solids*, 61 (2000) 1153-1158.
- [52] H. Chen, D.S. Sholl, Predictions of selectivity and flux for CH₄/H₂ separations using single walled carbon nanotubes as membranes, *Journal of Membrane Science*, 269 (2006) 152-160.
- [53] S. Majeed, D. Fierro, K. Buhr, J. Wind, B. Du, A. Boschetti-de-Fierro, V. Abetz, Multi-walled carbon nanotubes (MWCNTs) mixed polyacrylonitrile (PAN) ultrafiltration membranes, *Journal of Membrane Science*, 403-404 (2012) 101-109.
- [54] P.M. Budd, N.B. McKeown, B.S. Ghanem, K.J. Msayib, D. Fritsch, L. Starannikova, N. Belov, O. Sanfirova, Y. Yampolskii, V. Shantarovich, Gas permeation parameters and other physicochemical properties of a polymer of intrinsic microporosity: Polybenzodioxane PIM-1, *Journal of Membrane Science*, 325 (2008) 851-860.
- [55] I. Pinnau, L.G. Toy, Gas and vapor transport properties of amorphous perfluorinated copolymer membranes based on 2,2-bis(trifluoromethyl)-4,5-difluoro-1,3-dioxole/tetrafluoroethylene, *Journal of Membrane Science*, 109 (1996) 125-133.
- [56] N. Du, M.M. Dal-Cin, G.P. Robertson, M.D. Guiver, Decarboxylation-Induced Cross-Linking of Polymers of Intrinsic Microporosity (PIMs) for Membrane Gas Separation†, *Macromolecules*, 45 (2012) 5134-5139.
- [57] J.-P. Salvetat, A.J. Kulik, J.-M. Bonard, G.A.D. Briggs, T. Stöckli, K. Méténier, S. Bonnamy, F. Béguin, N.A. Burnham, L. Forró, Elastic Modulus of Ordered and Disordered Multiwalled Carbon Nanotubes, *Advanced Materials*, 11 (1999) 161-165.
- [58] H. Daniel Wagner, Nanotube-polymer adhesion: a mechanics approach, *Chemical Physics Letters*, 361 (2002) 57-61.
- [59] M.R. Loos, V. Abetz, K. Schulte, Dissolution of MWCNTs by using polyoxadiazoles, and highly effective reinforcement of their composite films, *Journal of Polymer Science Part A: Polymer Chemistry*, 48 (2010) 5172-5179.

Scheme 1:



Scheme 2:

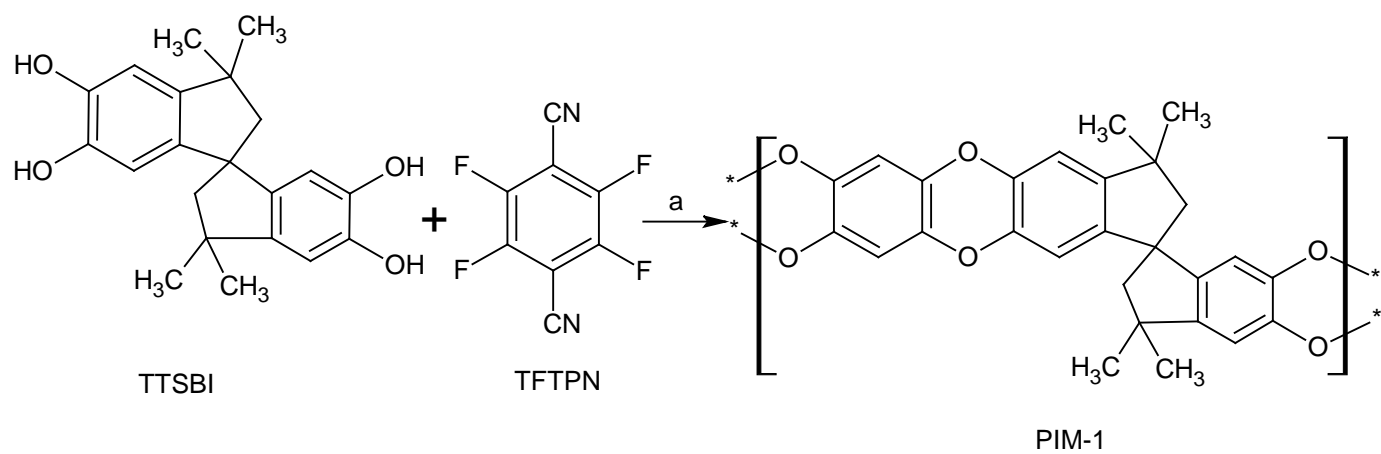


Figure 1:

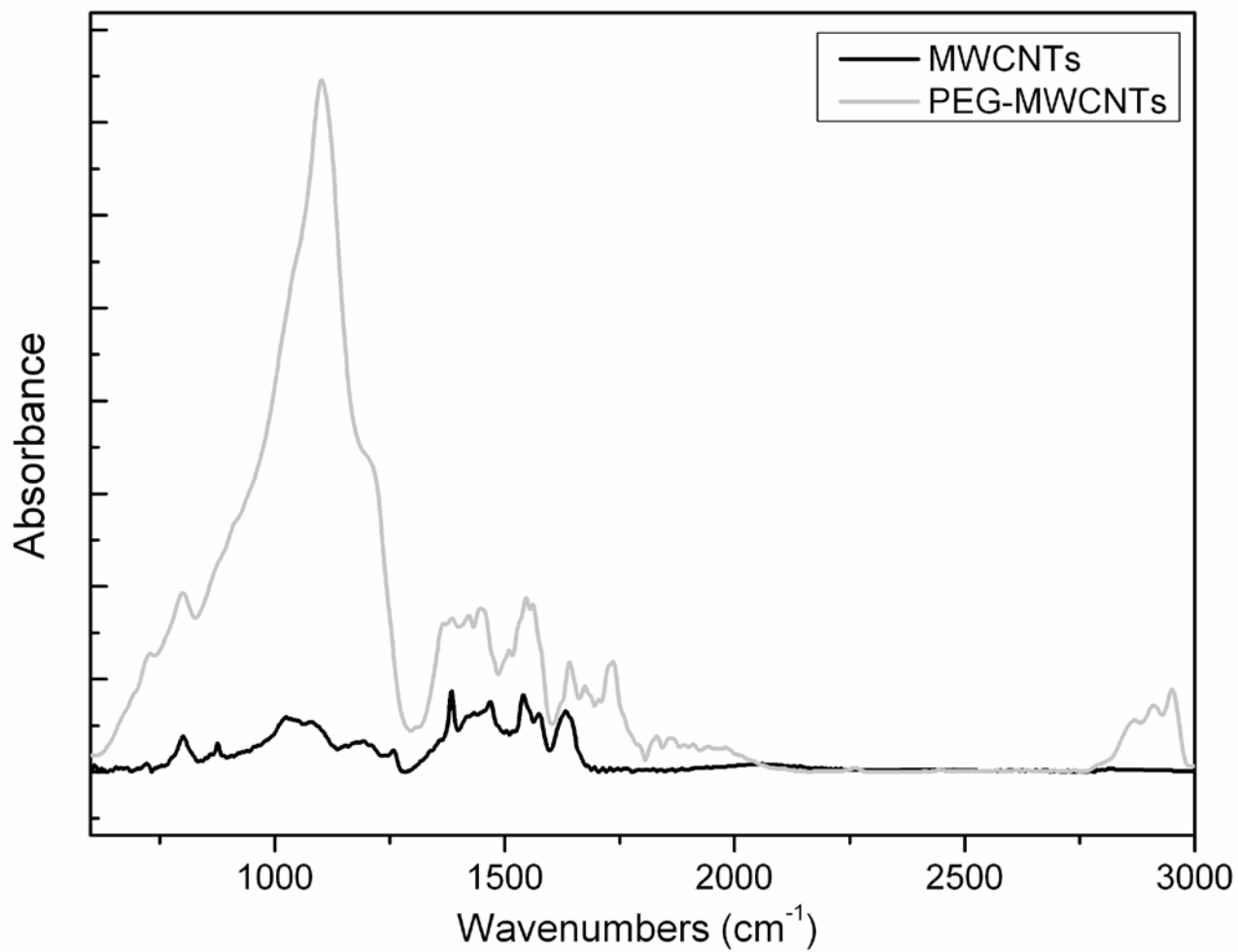


Figure 2:

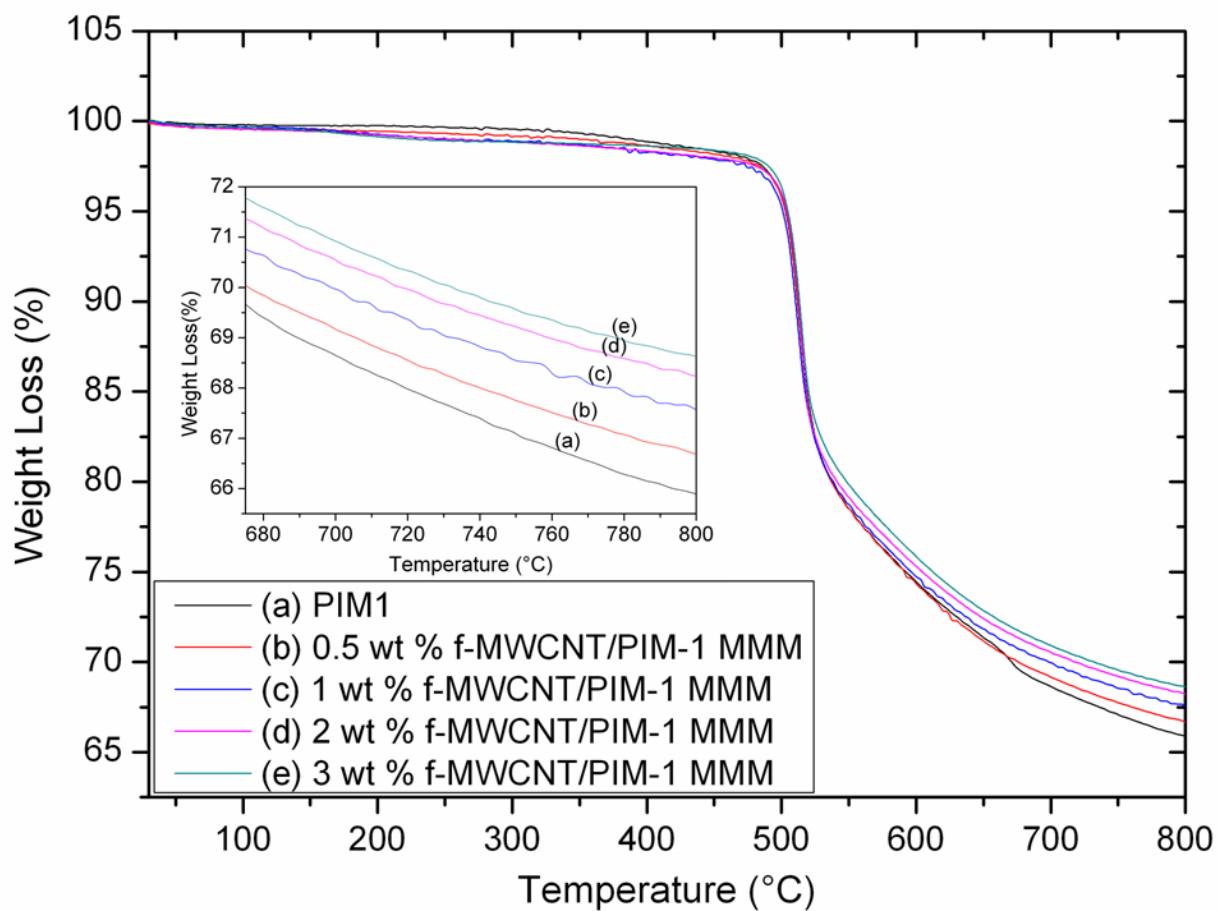


Figure 3:

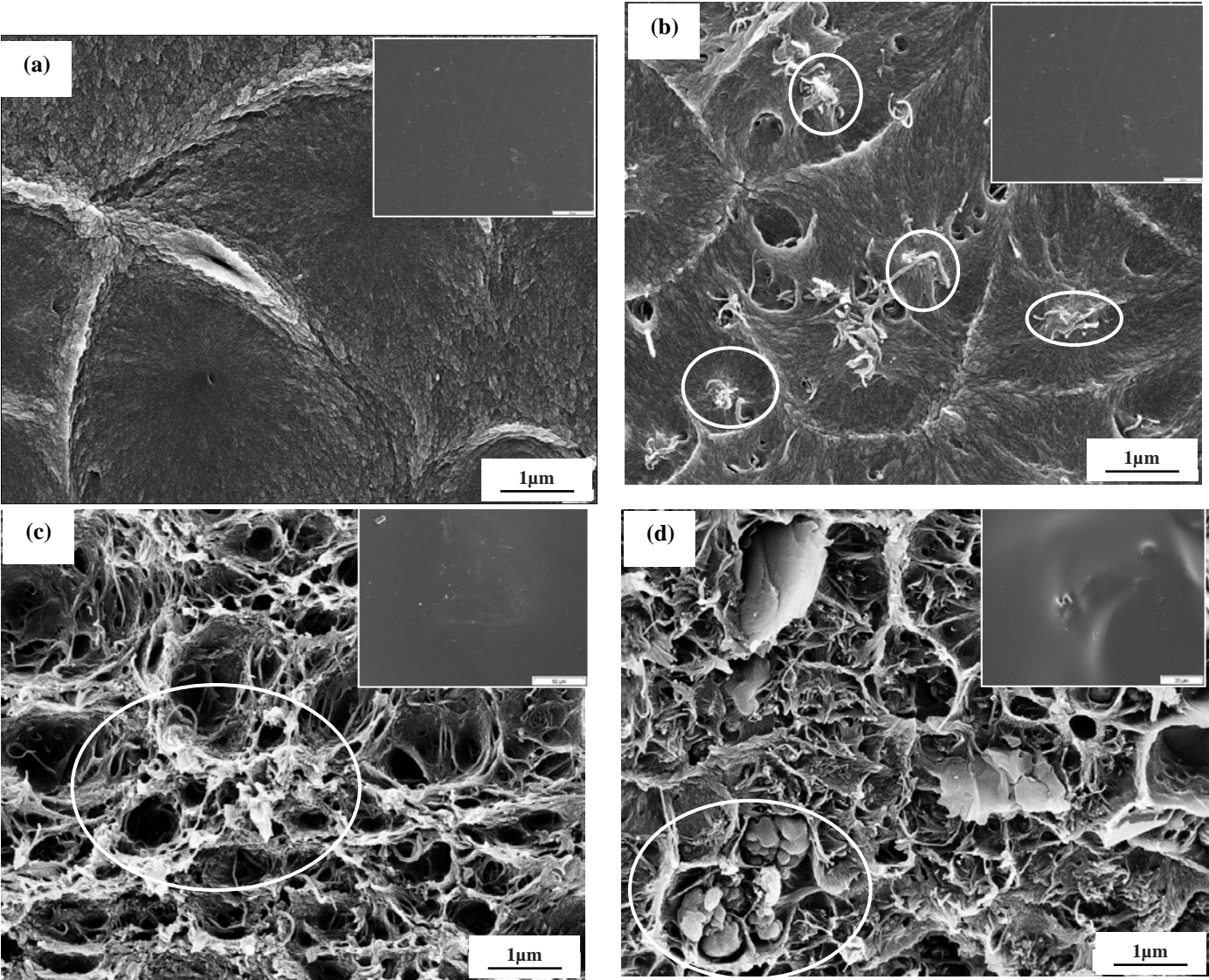


Figure 4:

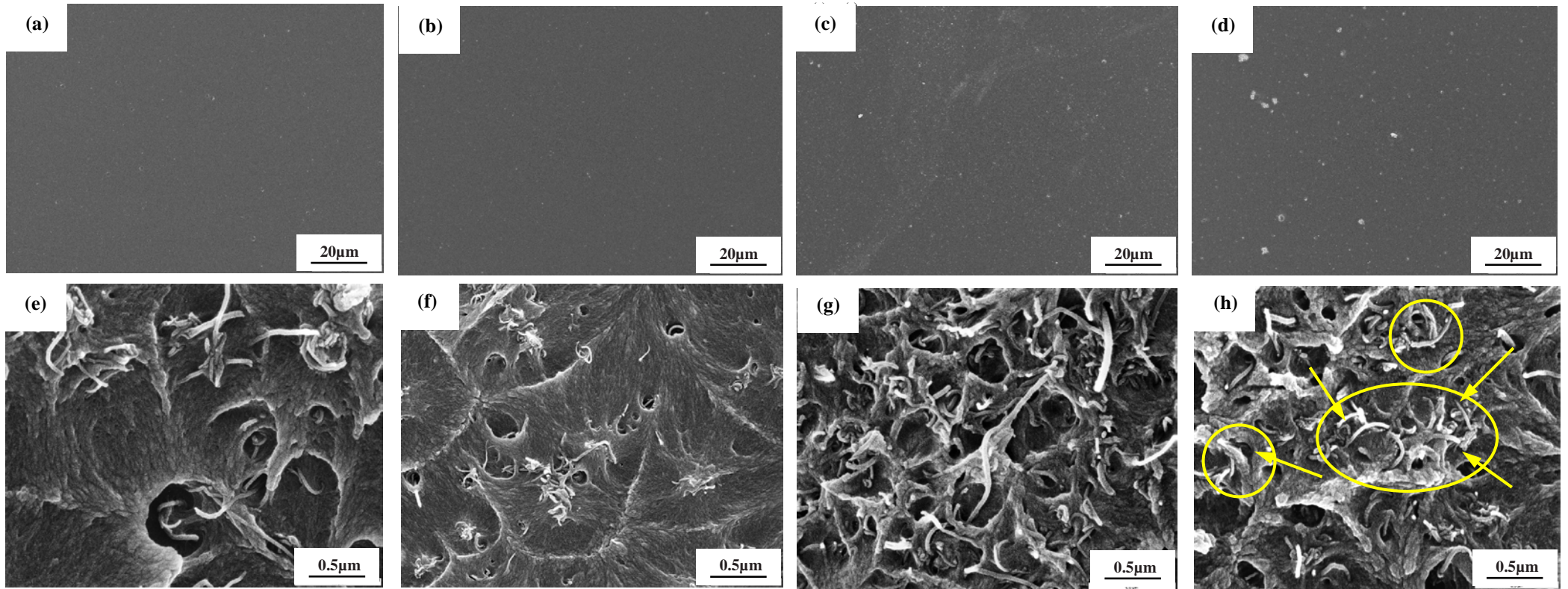


Figure 5:

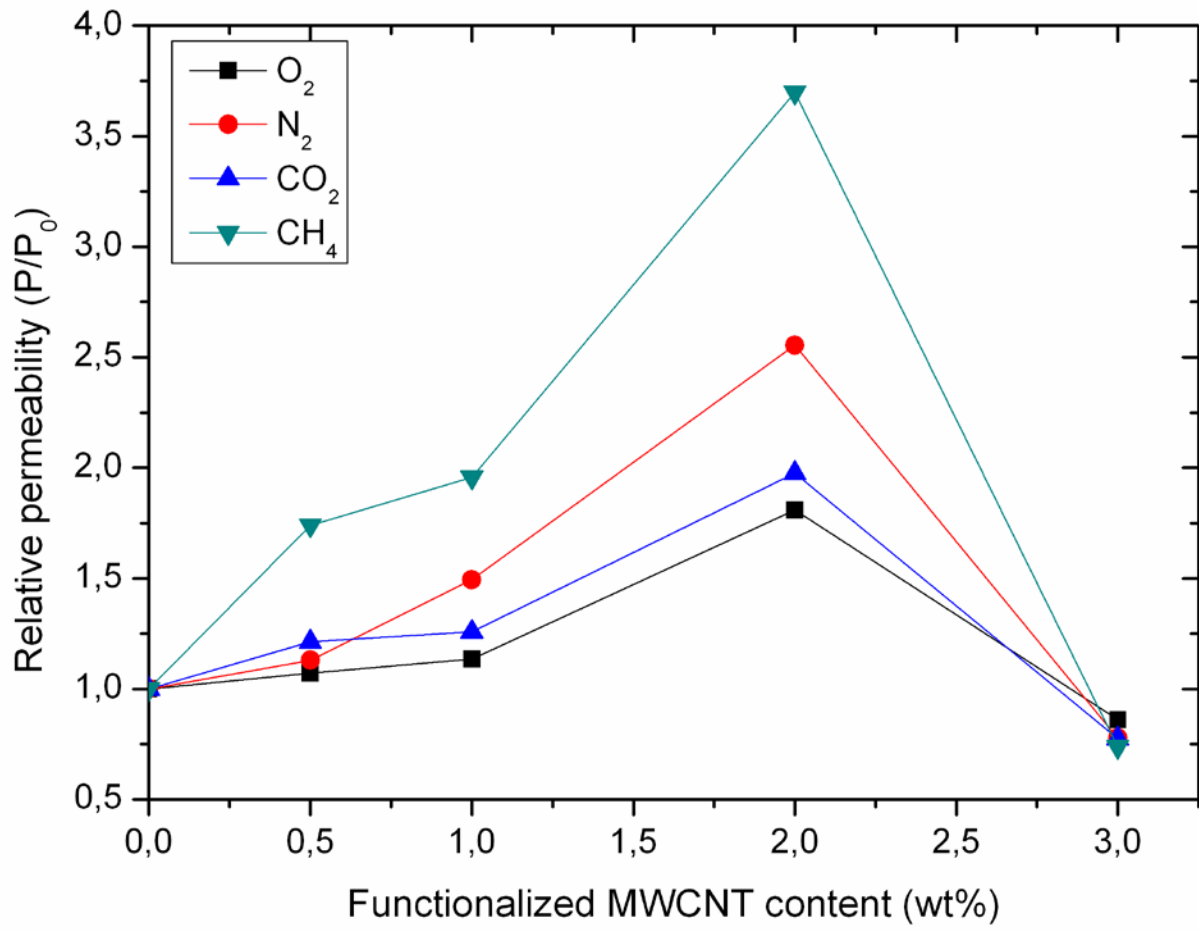


Figure 6:

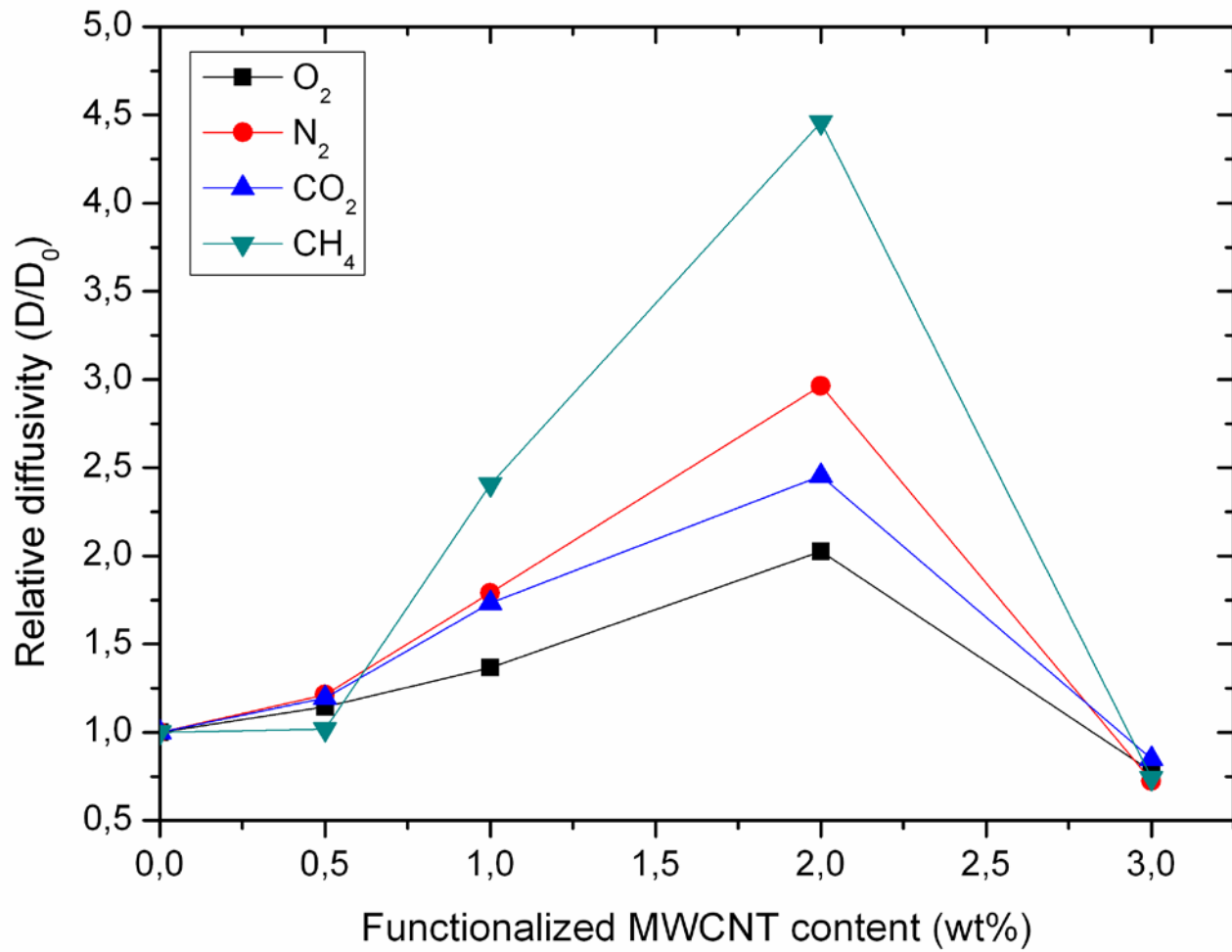


Figure 7:

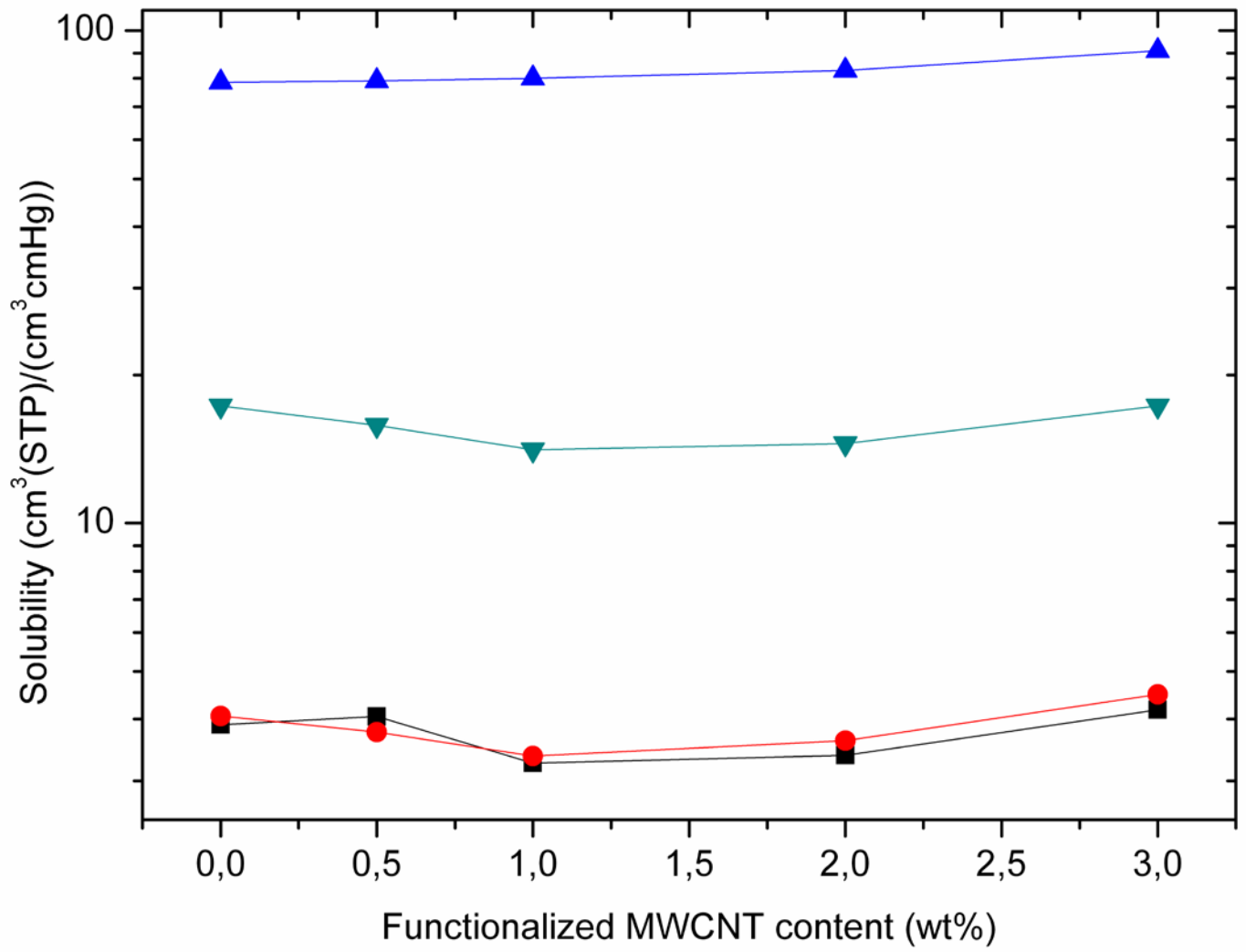


Figure 8 (a):

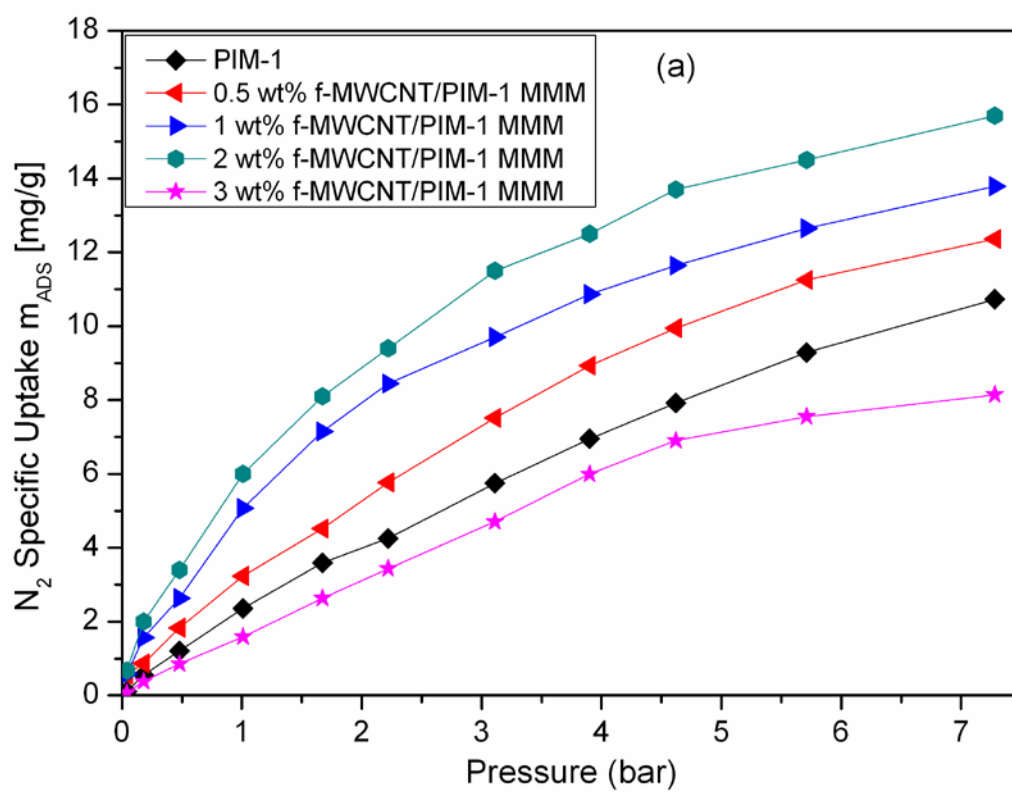


Figure 8 (b):

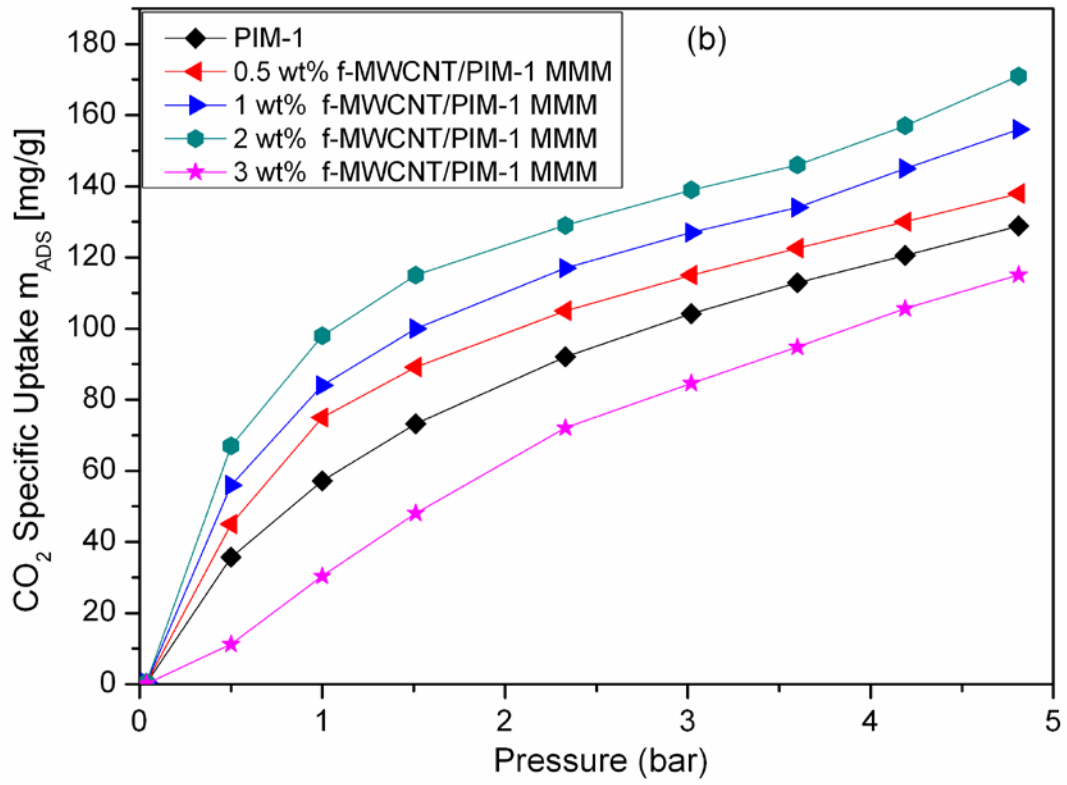


Figure 9:

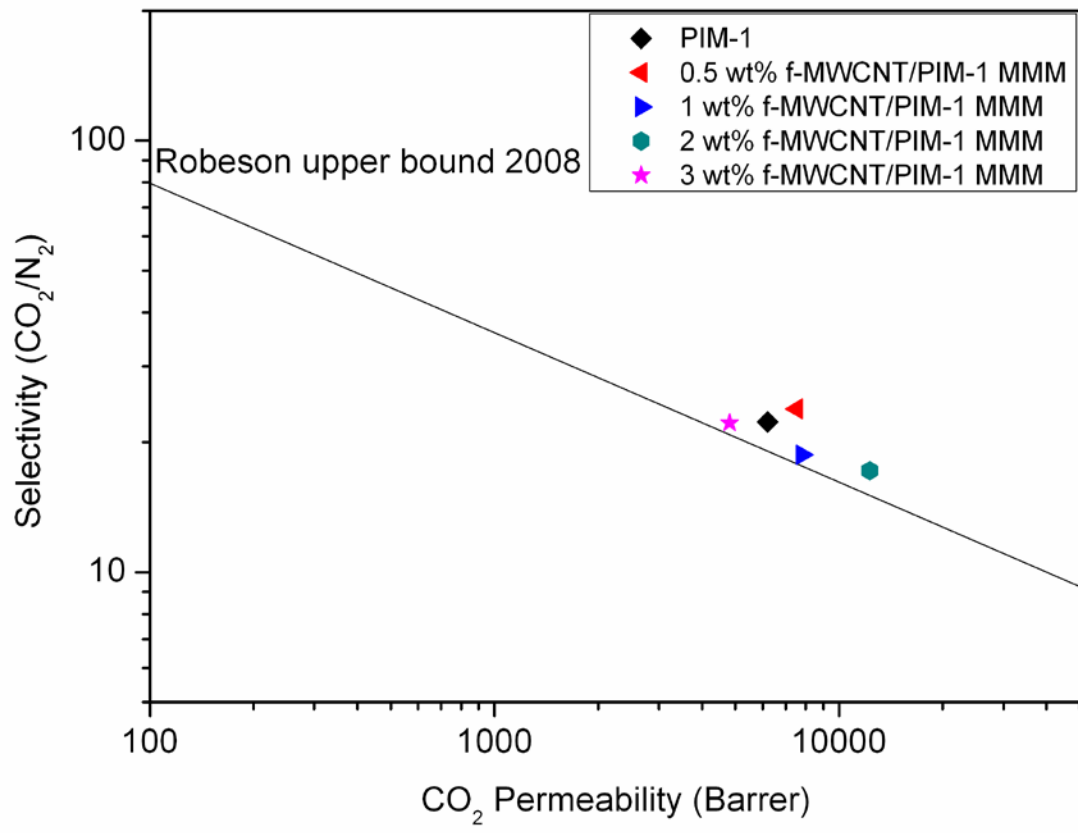


Figure 10:

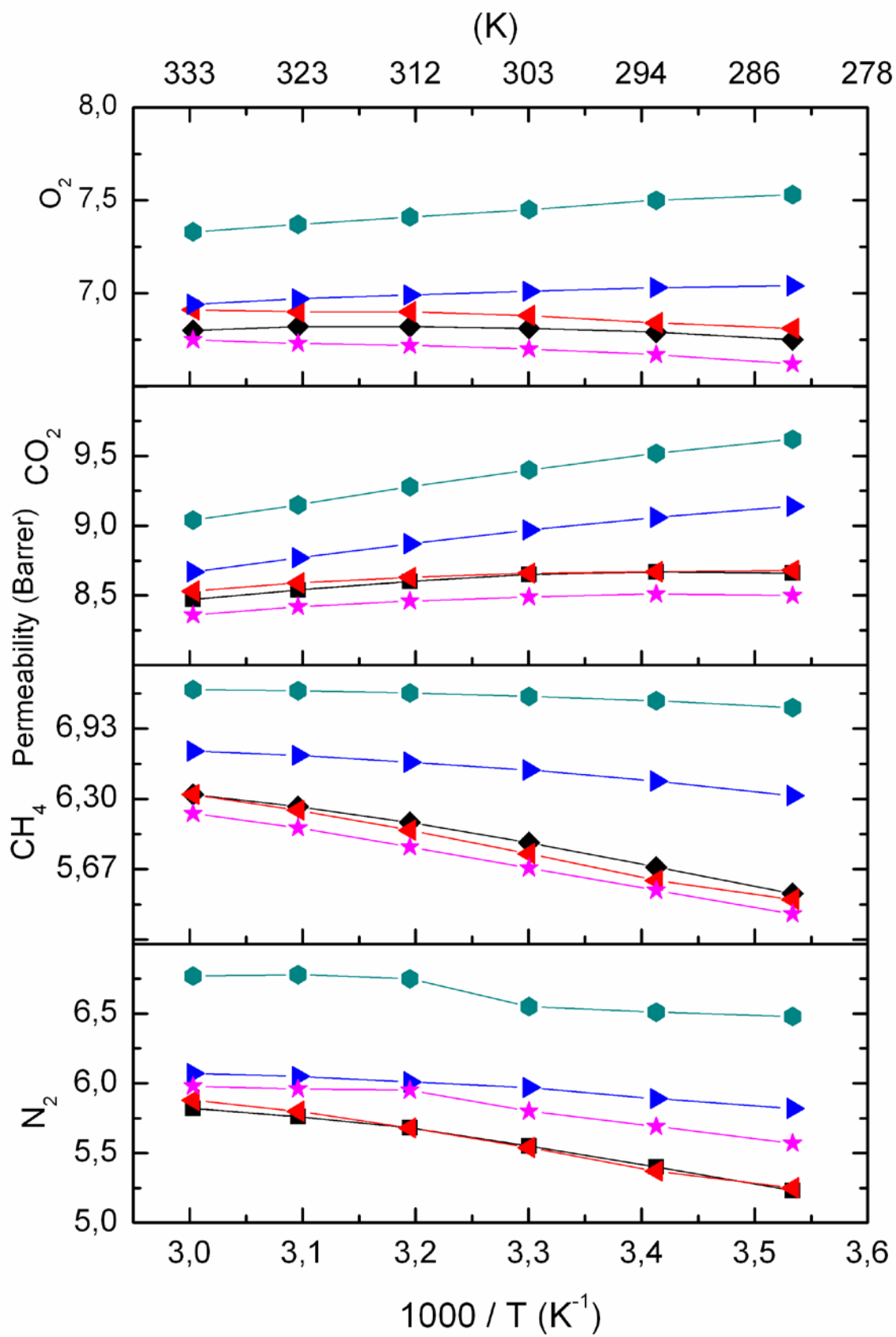


Figure 11:

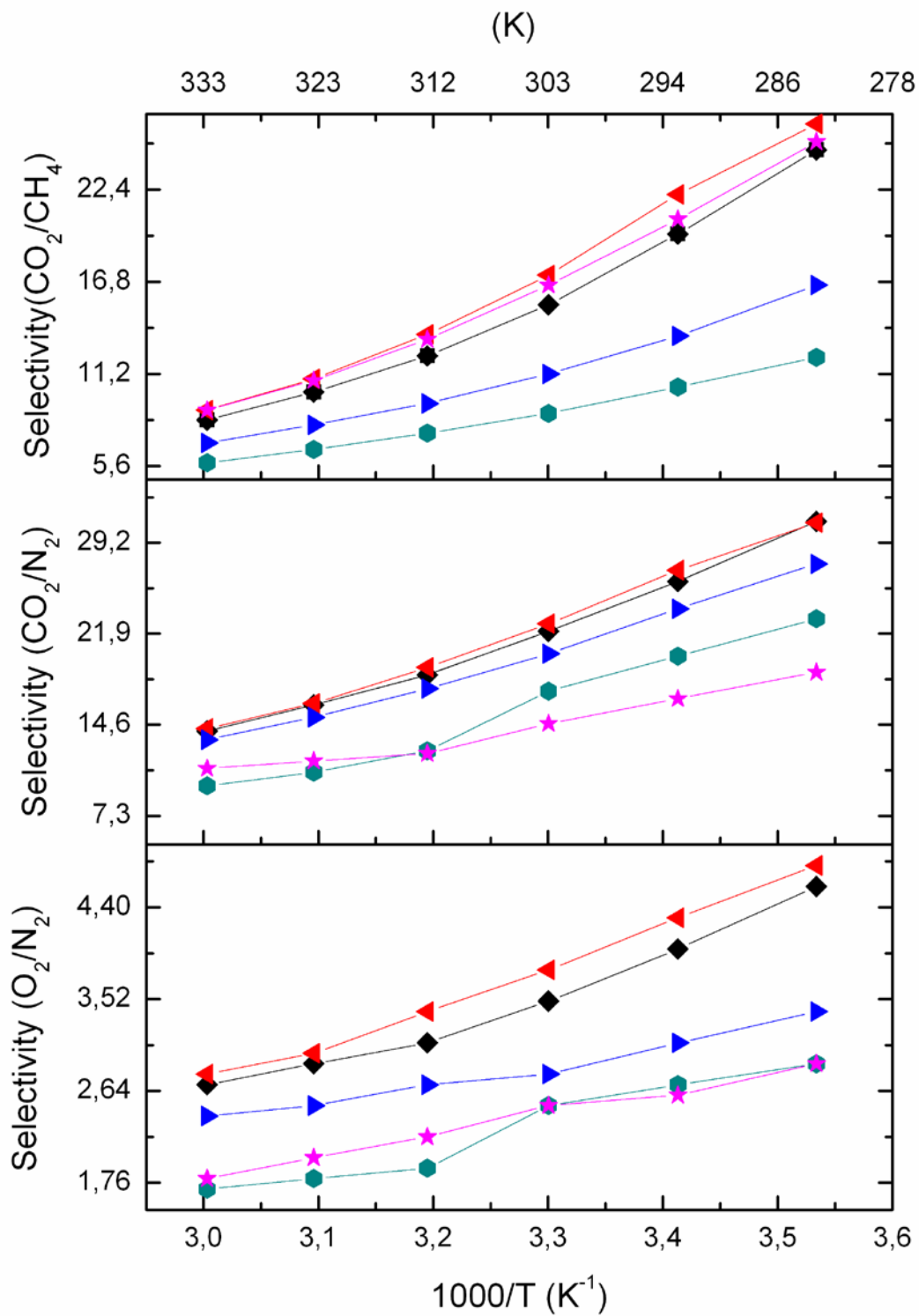


Figure 12 (a):

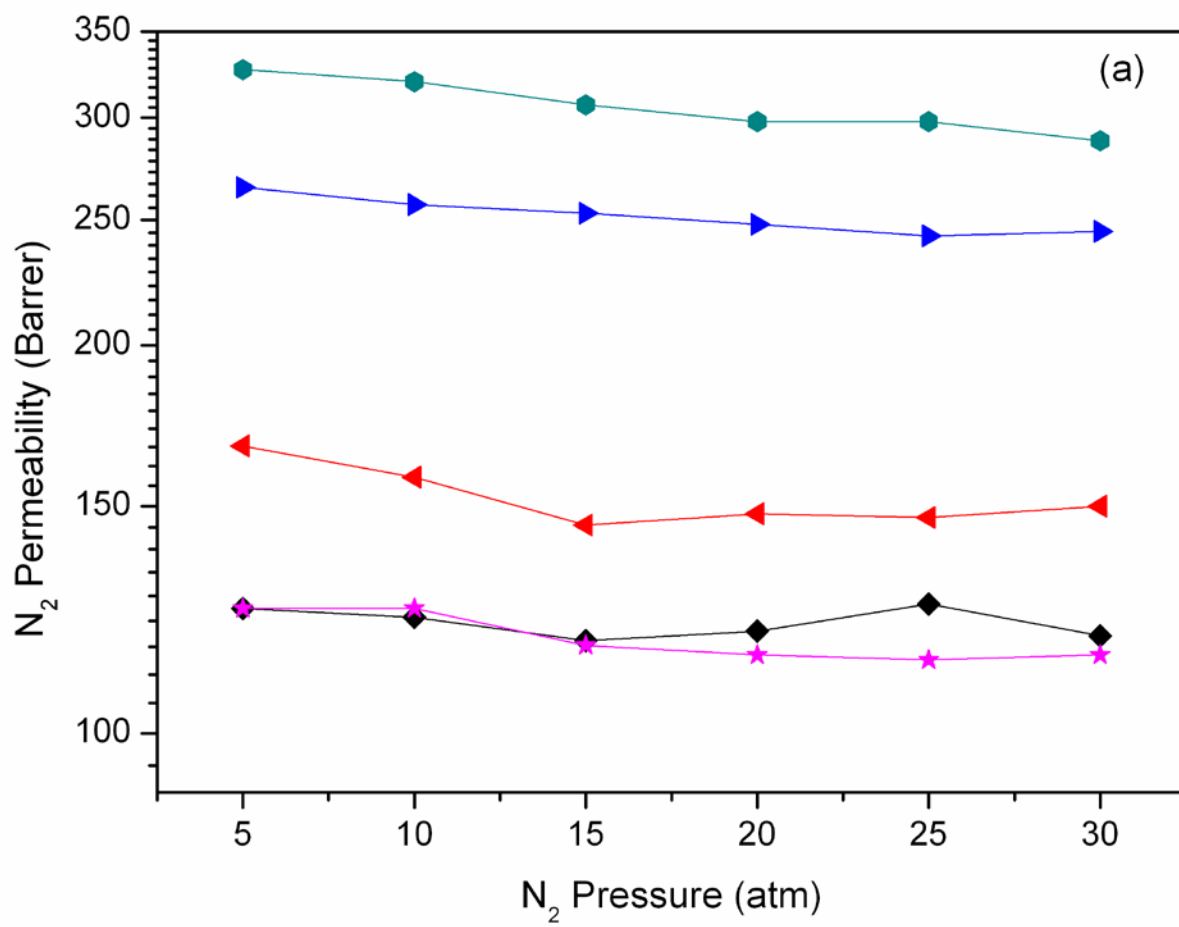


Figure 12 (b):

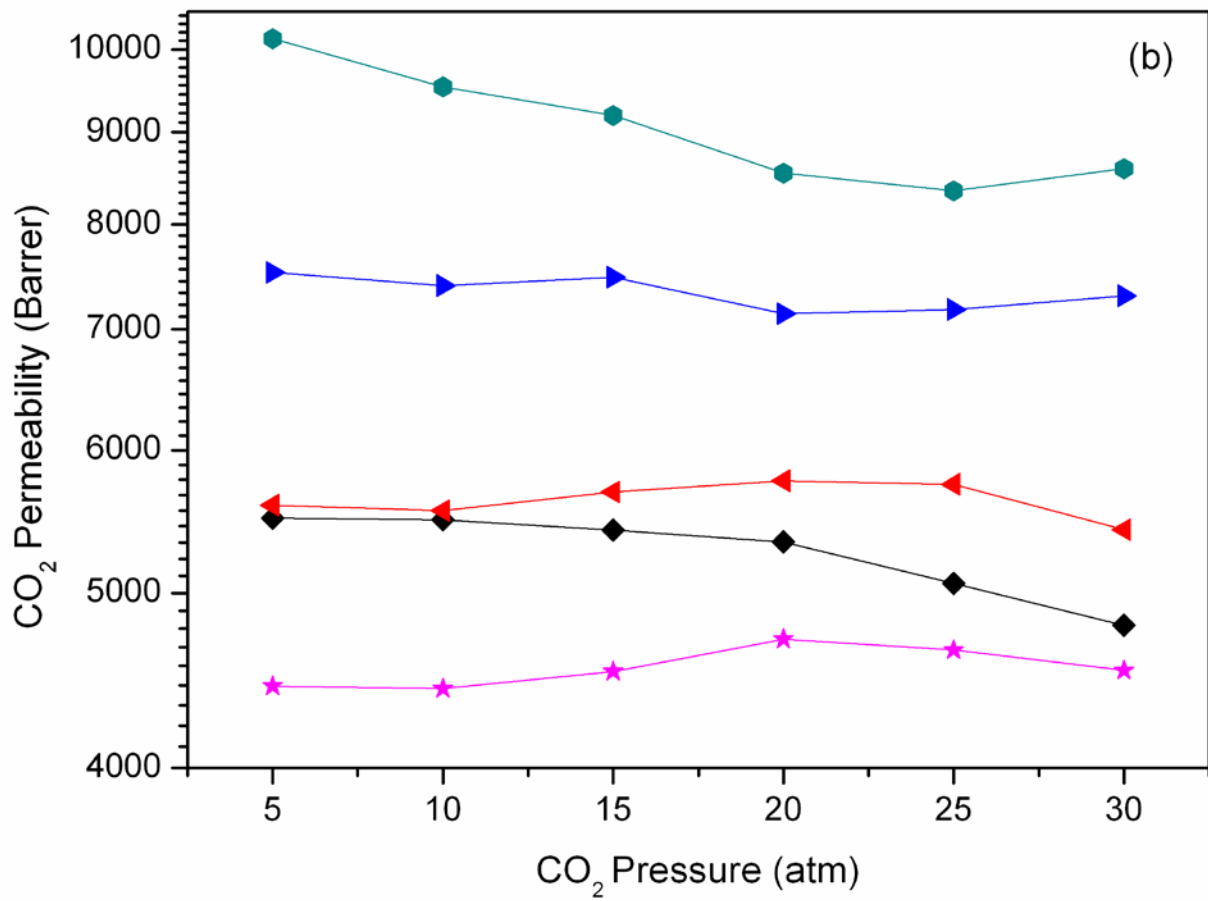


Figure 12 (c):

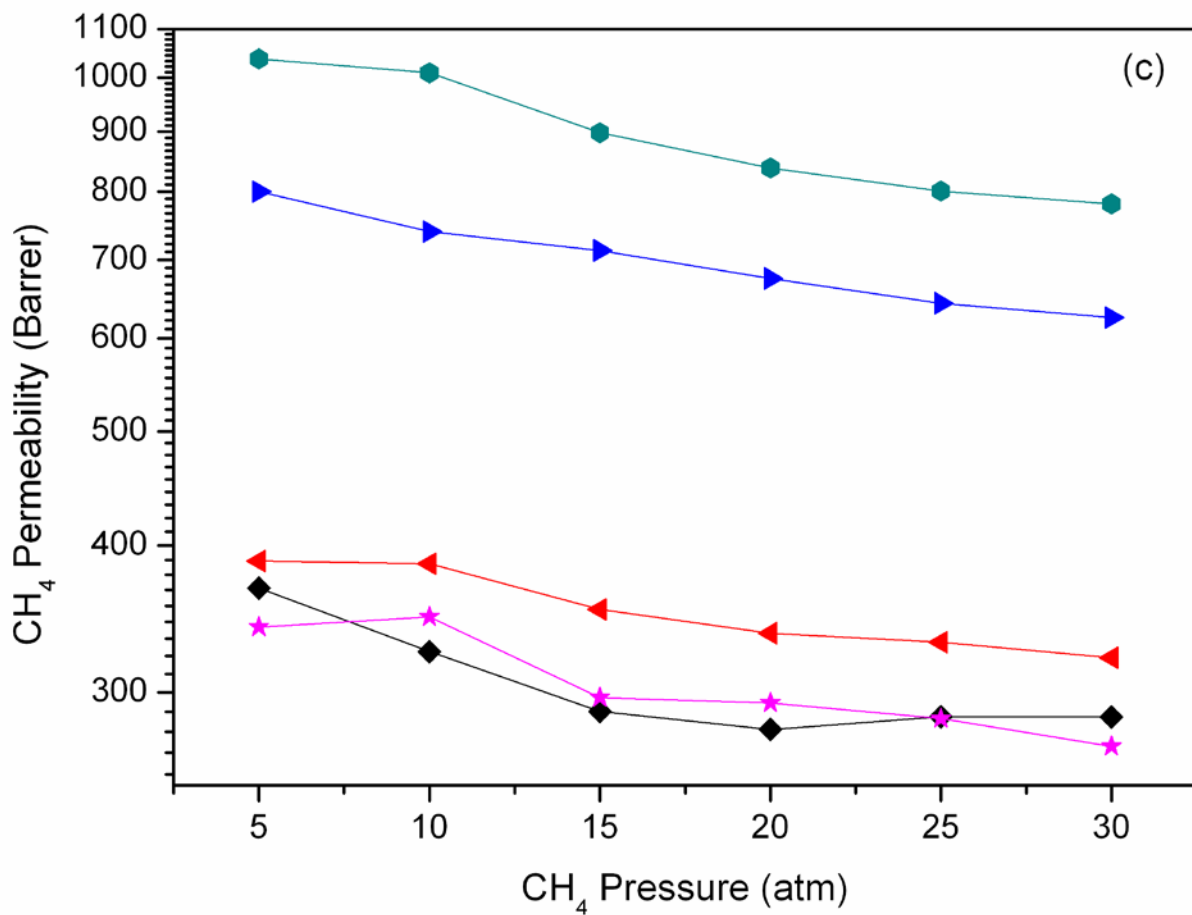


Table 1:

Membranes	Before methanol treatment		After methanol treatment	
	Thickness (μm)	Diameter (cm)	Thickness (μm)	Diameter (cm)
PIM-1	100.5 ± 4.6	4.65	109.4 ± 4.2	4.57
1 wt% SWCNTs/PIM-1 MMM	100.7 ± 3.7	4.65	112.5 ± 3.1	4.57
1 wt% MWCNTs/PIM-1 MMM	102.5 ± 3.1	4.65	111.9 ± 3.1	4.57
0.5 wt% f-MWCNTs/PIM-1 MMM	112.5 ± 3.1	4.65	121.7 ± 3.9	4.57
1 wt% f-MWCNTs/PIM-1 MMM	103.1 ± 4.0	4.65	113.4 ± 4.7	4.57
2 wt% f-MWCNTs/PIM-1 MMM	104.4 ± 4.1	4.65	117.5 ± 4.8	4.57
3 wt% f-MWCNTs/PIM-1 MMM	101.6 ± 4.8	4.65	115.1 ± 5.1	4.57

Table 2:

Membrane	Permeability (Barrer)				Selectivity		
	N ₂	O ₂	CO ₂	CH ₄	O ₂ /N ₂	CO ₂ /N ₂	CO ₂ /CH ₄
PIM-1	279	928	6211	401	3.3	22.2	15.5
1 wt % f-MWCNTs/PIM-1 MMM	417	1054	7813	785	2.5	18.7	9.9
1 wt% MWCNTs/PIM-1 MMM	361	957	6219	757	2.6	17.2	8.2
1 wt% SWCNTs/PIM-1 MMM	949	2305	15721	1820	2.4	16.5	8.6

$$1\text{Barrer} = 1 \times 10^{-10} \cdot \frac{\text{cm}^3_{(STP)} \cdot \text{cm}}{\text{cm}^2 \cdot \text{sec} \cdot \text{cmHg}}$$

Table 3:

Membrane	Permeability (Barrer)				
	He	N ₂	O ₂	CO ₂	CH ₄
PIM1	1048	279	928	6211	401
0.5 wt% f-MWCNT/PIM-1 MMM	1167 (11.35%)	315 (12.9%)	995 (7.22%)	7535 (21.32%)	698 (74.06%)
1 wt% f-MWCNT/PIM-1 MMM	1247 (18.98%)	417 (49.46%)	1054 (13.57%)	7813 (25.79%)	785 (95.76%)
2 wt% f-MWCNT/PIM-1 MMM	1355 (29.29%)	713 (255.55%)	1680 (181.03%)	12274 (197.61%)	1483 (369.82%)
3 wt% f-MWCNT/PIM-1 MMM	1050 (0.28%)	217 (-22.22%)	799 (-13.90%)	4816 (-22.46%)	296 (-26.18%)

(+ve) increment from pure polymer

(-ve) decrement from pure polymer

$$1\text{Barrer} = 1 \times 10^{-10} \cdot \frac{\text{cm}^3_{(STP)} \cdot \text{cm}}{\text{cm}^2 \cdot \text{sec} \cdot \text{cmHg}}$$

Table 4:

Membrane	N ₂	O ₂	CO ₂	CH ₄
PIM1	7.15	22.9	7.91	2.31
0.5 wt% f-MWCNT/PIM-1 MMM	8.68 (21.39%)	26.2 (14.41%)	9.45 (19.47%)	2.35 (1.73%)
1 wt% f-MWCNT/PIM-1 MMM	12.8 (79.02%)	31.3 (36.68%)	13.7 (73.19%)	5.56 (140.69%)
2 wt% f-MWCNT/PIM-1 MMM	21.2 (196.50%)	46.4 (102.62%)	19.4 (145.25%)	10.3 (345.88%)
3 wt% f-MWCNT/PIM-1 MMM	5.18 (-27.55%)	17.8 (-22.27%)	6.72 (-15.04%)	1.71 (-25.97%)

(+ve) increment from pure polymer

(-ve) decrement from pure polymer

Table 5:

Membrane	O ₂ /N ₂	CO ₂ /N ₂	CO ₂ /CH ₄	He/CH ₄
PIM-1	3.3	22.3	15.5	2.6
0.5 wt% f-MWCNT/PIM-1 MMM	3.2	23.9	10.8	1.7
1 wt% f-MWCNT/PIM-1 MMM	2.5	18.7	9.9	1.6
2 wt% f-MWCNT/PIM-1 MMM	2.4	17.2	8.3	0.9
3 wt% f-MWCNT/PIM-1 MMM	3.7	22.2	16.3	3.5

Table 6:

Membrane	E_p (kJ/mol)		
	N ₂	CH ₄	CO ₂
PIM-1	9.4	14.7	-3.1
0.5 wt% f-MWCNT/PIM-1 MMM	10.3	15.5	-2.2
1 wt% f-MWCNT/PIM-1 MMM	5.5	6.2	-7.4
2 wt% f-MWCNT/PIM-1 MMM	4.0	2.5	-1.0
3 wt% f-MWCNT/PIM-1 MMM	6.8	14.3	-2.2

Table 7:

Membrane	f-MWCNTs (wt %)	E^a (MPa)	σ_M^b (MPa)	ε^c (%)
PIM-1	0	530 ± 152	39 ± 4	6.1 ± 1
0.5 wt% f-MWCNT/PIM-1 MMM	0.5	626 ± 122	44 ± 6	6.2 ± 2
1 wt% f-MWCNT/PIM-1 MMM	1	666 ± 153	47 ± 7	8.2 ± 2
2 wt% f-MWCNT/PIM-1 MMM	2	685 ± 175	48 ± 6	8.9 ± 3
3 wt% f-MWCNT/PIM-1 MMM	3	640 ± 170	46 ± 6	8 ± 2

^a Young's modulus; ^b Tensile strength ; ^c Elongation at break

Schemes captions:

Scheme 1: Functionalization of pristine MWCNTs via 'grafting to' method

Scheme 2: Synthesis of PIM-1, a - Reagent and condition, K_2CO_3 , DMAc, DEB, 150 °C, 1 h

Figures captions:

Fig.1: Infrared spectra of MWCNT and PEG grafted MWCNT.

Fig.2: TGA of the pure PIM-1 and f-MWCNTs/PIM-1 MMM.

Fig.3: SEM images of surface (inset) and cross section of PIM-1 (a), PIM-1 MMM incorporated with 1 wt% of f-MWCNTs (b), pristine MWCNTs (c) and pristine SWCNTs (d).

Fig.4: SEM images of surface and cross section of PIM-1 MMM incorporated with different f-MWCNT loading : 0.5 wt% (a)-(e) ; 1 wt% (b)-(f) ; 2 wt% (c)-(g) and 3 wt% (d)-(h).

Fig.5: Relative permeability (i.e. ratio of permeability of f-MWCNTs/PIM-1 with pure polymer) of f-MWCNTs/PIM-1 MMM to a variety of penetrants as a function of f-MWCNTs content at 30°C

Fig.6: Relative diffusivity (i.e. ratio of permeability of f-MWCNTs/PIM-1 with pure polymer) of f-MWCNTs/PIM-1 MMM to a variety of penetrates as a function of f-MWCNTs content at 30 °C.

Fig.7: Solubility coefficient of f-MWCNTs/PIM-1 MMM to a variety of penetrants as a function of f-MWCNTs content at 30°C by time-lag method [O_2 (■), N_2 (●), CO_2 (▲)] CH_4 (▼),.

Fig.8: Adsorption isotherms on PIM-1, 0.5wt %, 1 wt%, 2 wt%, 3 wt% functionalized MWCNTs/PIM-1 MMMs. (a) N_2 (b) CO_2 .

Fig.9: Trade-off between CO_2 permeability and CO_2/N_2 selectivity of PIM-1 and f-MWCNTs/PIM-1 MMM relative to the Robeson upper bound line.

Fig.10: Permeability of N_2 , CH_4 , CO_2 , O_2 in PIM-1 and f-MWCNT/PIM-1 MMM as a function of reciprocal temperature [(♦) PIM-1, (◄) 0.5 wt% f-MWCNT/PIM-1 MMM, (►) 1 wt% f-MWCNT/PIM-1 MMM, (●) 2 wt% f-MWCNT/PIM-1 MMM, (★) 3 wt% f-MWCNT/PIM-1 MMM].

Fig.11: Selectivity of O_2/N_2 , CO_2/N_2 , CO_2/CH_4 , in PIM-1 and f-MWCNT/PIM-1 MMM as a function of reciprocal temperature [(♦) PIM-1, (◄) 0.5 wt% f-MWCNT/PIM-1 MMM, (►) 1 wt% f-MWCNT/PIM-1 MMM, (●) 2 wt% f-MWCNT/PIM-1 MMM, (★) 3 wt% f-MWCNT/PIM-1 MMM].

Fig.12: Permeability of (a) N_2 , (b) CO_2 , and (c) CH_4 , in PIM-1 and f-MWCNT/PIM-1 MMM as a function of different feed pressures [(♦) PIM-1, (◄) 0.5 wt% f-MWCNT/PIM-1 MMM, (►) 1 wt% f-MWCNT/PIM-1 MMM, (●) 2 wt% f-MWCNT/PIM-1 MMM, (★) 3 wt% f-MWCNT/PIM-1 MMM].

Table captions:

Table 1: Thickness and diameter of pure PIM-1 and f-MWCNTs/PIM-1 MMM

Table 2: Gas permeabilities (Barrer) and selectivity of various gas pairs in pure PIM-1, 1 wt% f-MWCNTs/PIM1 MMM, 1 wt% SWCNTs/PIM-1 MMM and 1 wt % MWCNTs/PIM1 MMM

Table 3: Gas permeabilities (Barrer) of various gases in pure PIM-1 and f-MWCNT/PIM-1 MMM

Table 4: Diffusivity (10^{-7} cm²/sec) of various gases in the pure PIM1 and f-MWCNTs/PIM-1 MMM

Table 5: Selectivity of various gas pairs for pure PIM-1 and f-MWCNTs/PIM-1 MMM

Table 6: Activation energy of permeation for pure PIM-1 and f-MWCNTs/PIM-1 MMM

Table 7: Summary of tensile test results of pure PIM-1 and f-MWCNTs/PIM-1 MMM